Precambrian Research 299 (2017) 15–33

Contents lists available at ScienceDirect

Precambrian Research

journal homepage: www.elsevier.com/locate/precamres

# New zircon U–Pb and Hf–Nd isotopic constraints on the timing of magmatism, sedimentation and metamorphism in the northern Prince Charles Mountains, East Antarctica

Xiaochun Liu [a,*], Yue Zhao [a], Hong Chen [a], Biao Song [b]

[a] Institute of Geomechanics, Chinese Academy of Geological Sciences, Beijing 100081, China
[b] Beijing SHRIMP Centre, Institute of Geology, Chinese Academy of Geological Sciences, Beijing 100037, China

ARTICLE INFO

*Article history:*
Received 17 April 2017
Revised 10 July 2017
Accepted 13 July 2017
Available online 15 July 2017

*Keywords:*
Zircon
Magmatic age
Depositional age
Metamorphic age
Rayner orogen
East Antarctica

ABSTRACT

The northern Prince Charles Mountains (PCM) in East Antarctica represent the largest continuously exposed section of the Rayner Complex and may provide important insights into the tectonic evolution of the Rayner orogen. We present new U–Pb and Hf isotopic data for zircons from felsic orthogneisses, mafic granulites, paragneisses and charnockites and additional Nd isotopic data for the former two rock types from the Beaver Lake area in the northern PCM. Zircons from the felsic orthogneisses document protolith ages of ca. 1170–1070 Ma, with Hf and Nd model ages of 1.99–1.74 Ga, suggesting the generation of the felsic magmas by partial melting of crustal rocks that were extracted from the mantle during the Paleoproterozoic. Detrital zircons from one paragneiss sample yield a major age population at ca. 1480–1140 Ma and three subordinate populations at ca. 2130–1850, 1780–1620 and 1010–860 Ma, whereas those from another paragneiss sample produce a major age population at ca. 1180–830 Ma and a subordinate age population at ca. 1370–1230 Ma. Discounting the effects of zircon recrystallization during post-depositional metamorphism, we infer that the sedimentary precursors to the aforementioned paragneiss samples were deposited after ca. 1200 and 1020 Ma, respectively, in intra- or back-arc basins of the Rayner continental arc. Charnockites were either emplaced at ca. 980 Ma or episodically at ca. 1050 and ca. 950 Ma, with Hf model ages of 1.97–1.90 Ga. They were derived from partial melting of a Paleoproterozoic source region similar to the surrounding felsic orthogneisses at deeper levels. Zircon overgrowth domains from all of the studied rock types indicate that high-grade metamorphism took place at ca. 945–915 Ma. Only one paragneiss sample from the Else Platform preserves evidence of Cambrian metamorphic reworking. Based on published data from the Rayner Complex and the Eastern Ghats Belt of India, we speculate that long-lived convergent processes between the Indian craton and East Antarctica lasted from ca. 1500 to 900 Ma. Therefore, the Rayner Complex may represent the exposed orogenic root of a large Meso-Neoproterozoic accretionary orogen.



## 1. Introduction

The Rayner orogen, which formed between the Indian craton and East Antarctica, represents one of the largest known Meso-Neoproterozoic (i.e., Grenvillian) orogens. The orogen includes two main segments, namely the Rayner Complex in East Antarctica and the Eastern Ghats Belt (EGB) in India (Fig.1a). The Antarctic extent of the orogen may be more than 2000 km, from Enderby Land in the west to Queen Mary Land in the east, with a maximum width of >500 km (Black et al., 1987; Fitzsimons, 2000; Mikhalsky et al., 2015; Liu et al., 2016). The best exposures of the Rayner Complex occur in the well-studied northern Prince Charles Mountains (PCM)–Prydz Bay region. Earlier research for this region is mainly concerned with the discrimination of late Mesoproterozoic/early Neoproterozoic and late Neoproterozoic/Cambrian (i.e., Pan-African) high-grade tectonothermal events and the dating and *P*–*T* modeling of each event (e.g. Clarke et al., 1989; Manton et al., 1992; Zhao et al., 1992; Fitzsimons and Harley, 1994; Hand et al., 1994a; Hensen and Zhou, 1995; Carson et al., 1996, 2000; Fitzsimons et al., 1997; Kinny et al., 1997; Stephenson and Cook, 1997; Boger et al., 2000; Boger and White, 2003; Kelsey et al., 2003). During the last decade, investigations into the timing and processes of arc accretion prior to the main metamorphic episodes were undertaken in the area east of the Lambert Graben (Liu et al.,

* Corresponding author at: Institute of Geomechanics, Chinese Academy of Geological Sciences, 11 Minzudaxue Nanlu, Beijing 100081, China.
*E-mail address:* liuxchqw@cags.ac.cn (X. Liu).

http://dx.doi.org/10.1016/j.precamres.2017.07.012
0301-9268/

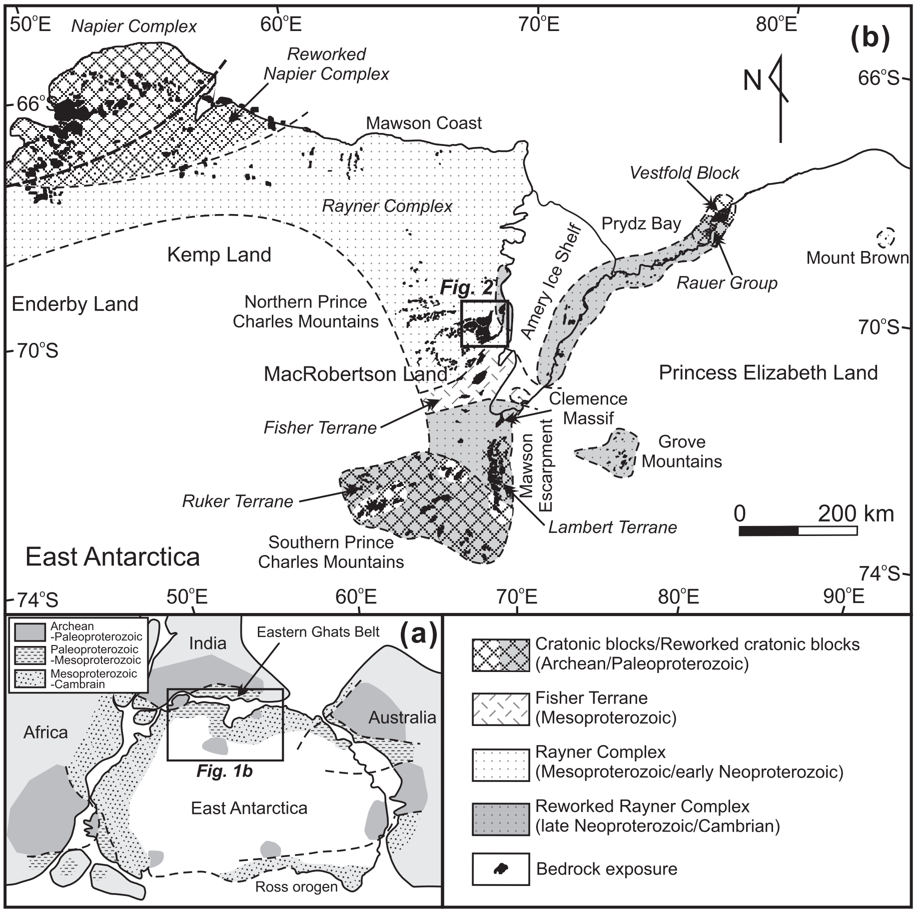


**Fig. 1.** Geological sketch map of the Indian Ocean sector of Antarctica (modified after Mikhalsky et al., 2001; Fitzsimons, 2003; Liu et al., 2016) with inset showing the location of the region in the reconstruction of Gondwana at ca. 500 Ma (modified after Hokada et al., 2016).

2007a, 2009, 2014, 2016; Wang et al., 2008; Grew et al., 2012, 2013; Mikhalsky et al., 2013). In contrast, the timing of magmatic activity in the northern PCM has received relatively little attention, except a few U–Pb zircon ages of ca. 1070–1020 Ma were obtained by some workers (Boger et al., 2000; Kamenev et al., 2009; Mikhalsky and Sheraton, 2011). On the other hand, more recent in situ U–Pb monazite dating for metapelites from the northern PCM yield significantly different age spectra for the high-grade metamorphism than those previously reported (Morrissey et al., 2015, 2016). These inconsistencies justify a renewed geochronological study of the basement rocks in the northern PCM.

In this contribution, we present new U–Pb zircon age data and Lu–Hf isotopic compositions for various metamorphic rocks and charnockites and Sm–Nd isotopic compositions for felsic orthogneisses and mafic granulites from the Beaver Lake area of the northern PCM. We attempt to establish a geochronological framework for the Meso-Neoproterozoic Rayner orogen in the northern PCM and further aim to address several specific issues: (1) the age and significance of a voluminous mafic-felsic magmatic event that occurred prior to the main episode of metamorphism; (2) the timing and provenance of the metasedimentary precursors in the northern PCM; (3) whether or not the charnockites were emplaced episodically, as was the case for the Mawson charnockite (Halpin et al., 2012); (4) whether or not the late Mesoproterozoic/early Neoproterozoic high-grade metamorphism was continuous between ca. 1000 and 900 Ma (e.g., Carson et al., 2000; Boger et al., 2000), or episodic (e.g., Liu et al., 2009, 2014); and (5) the response of zircons to late Neoproterozoic/Cambrian high-temperature metamorphic reworking. Our results, coupled with existing data from the same and adjacent areas, confirm the comparability of geological events on either side of the Lambert Graben and provide new constraints on the long-lived evolution of the Rayner orogen.

## 2. Regional geology

The Indian Ocean sector of Antarctica comprises five Archean/Paleoproterozoic cratonic blocks, the Mesoproterozoic Fisher Terrane and the Meso-Neoproterozoic Rayner Complex (Fig.1b). The Archean/Paleoproterozoic blocks include the Napier Complex in the Napier–Tula–Scott Mountains, the Ruker Terrane in the southern PCM, the Lambert Terrane in the northern Mawson Escarpment, and the Rauer Group (i.e., the Mather Terrane) and the Vestfold Block in Prydz Bay. Each of these blocks has its own distinct crustal history and they are therefore unlikely to represent the remnants of a single unified craton (Harley, 2003; Boger, 2011). The Fisher Terrane in the southern sector of the northern PCM consists mainly of 1300–1020 Ma mafic–felsic volcanics and intrusives that underwent amphibolite facies metamorphism at 1020–940 Ma (Beliatsky et al., 1994; Mikhalsky et al., 1996, 1999, 2001; Kinny et al., 1997). The Rayner Complex extends from Enderby Land eastwards to Kemp Land, MacRobertson Land and Princess Elizabeth Land. It includes 1490–1020 Ma mafic–felsic igneous rocks and coeval or younger sedimentary rocks that record regional granulite facies metamorphism accompanied by widespread charnockitic and granitic magmatism at ca. 1000–900 Ma (Black et al., 1987; Manton et al., 1992; Kinny et al., 1997; Boger et al., 2000; Carson et al., 2000; Kelly et al., 2002; Halpin et al., 2007a, 2013; Wang et al., 2008; Liu et al., 2009, 2014, 2016; Morrissey et al., 2015). To the east of the Lambert Graben, the Rayner Complex preserves evidence of pervasive reworking during a later Neoproterozoic/Cambrian high-grade tectonothermal event (Zhao et al., 1992; Hensen and Zhou, 1995; Fitzsimons et al., 1997; Liu et al., 2007a). This event also affected the Lambert and Ruker terranes, but metamorphism in these areas is limited to the greenschist and amphibolite facies (Boger and Wilson, 2005; Phillips et al., 2007).

The Rayner Complex in the northern PCM is exposed mainly in the Beaver Lake area, the Aramis, Porthos and Athos ranges, and some surrounding nunataks, covering a total area of ~40,000 km$^2$ (Fitzsimons and Thost, 1992). The main components of the complex in the Beaver Lake area (Fig. 2) are: (i) felsic orthogneisses derived mainly from pre- and *syn*-tectonic granitoids; (ii) mafic and occasional ultramafic granulites of intrusive igneous origin; (iii) metasedimentary rocks, including calc-silicates, pelites and semipelites; and (iv) late- and post-tectonic granitic intrusives, including charnockites, granites and various pegmatites (Stephenson, 2000). The structural evolution of the Rayner Complex appears to be consistent throughout the northern PCM (e.g., McKelvey and Stephenson, 1990; Fitzsimons and Thost, 1992; Hand et al., 1994b; Boger et al., 2000). Neoproterozoic deformation in response to continuous north–south directed compression evolved through several discrete phases (see the summary by Boger et al., 2000). Regionally extensive magmatism, peak metamorphism and subhorizontal shearing and recumbent folding occurred at ca. 990 Ma. Subsequent upright folding and shear zone development occurred at ca. 940–910 Ma. The main metamorphic episode reached medium- to low-pressure granulite-facies conditions (800–900 °C and 5–7 kbar) and was followed by near-isobaric cooling (Clarke et al., 1989; Fitzsimons and Harley, 1992, 1994; Thost and Henson, 1992; Hand et al., 1994a; Nichols, 1995; Scrimgeour and Hand, 1997; Stephenson and Cook, 1997; Boger and White, 2003; Morrissey et al., 2015). Late Neoproterozoic/Cambrian reworking was previously thought to be discrete, being defined by the formation of low-angle mylonites and pseudotachylites that accompanied by greenschist-amphibolite facies metamorphism and pegmatite intrusion (Fitzsimons and Thost, 1992; Manton et al., 1992; Carson et al., 2000; Boger et al., 2002). However, a more recent study suggests that this reworking may also have reached higher temperature grades, with *P–T* conditions of 800–870 °C and 5.5–6.5 kbar (Morrissey et al., 2016).

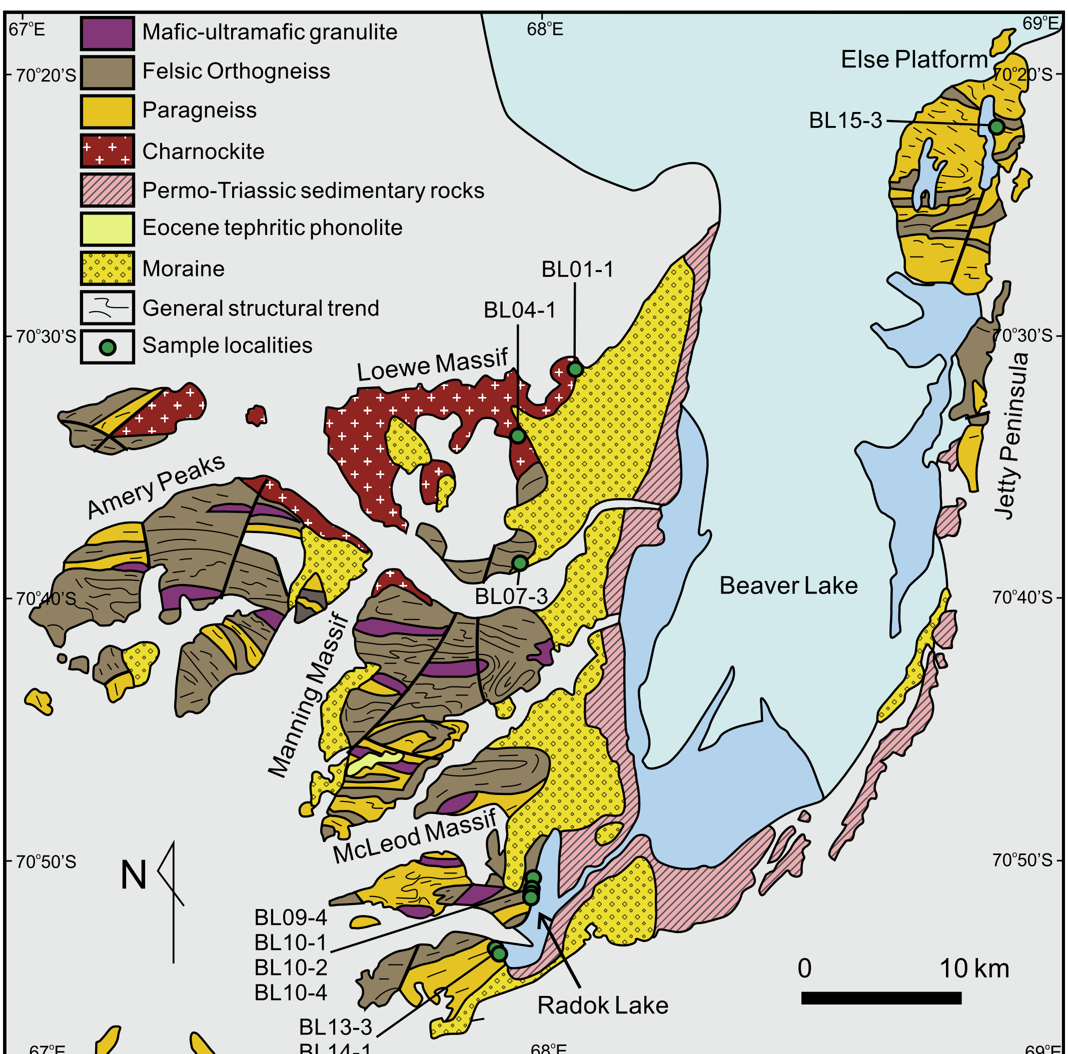


**Fig. 2.** Geological sketch map of the Beaver Lake area in the northern Prince Charles Mountains (modified after Mikhalsky et al., 2001) showing the localities of the studied samples.

## 3. Samples and analytical procedures

### 3.1. Sample descriptions

To precisely define ages of magmatism, sedimentation and metamorphism in the northern PCM, 10 samples of various rock types collected from the Beaver Lake area, including 4 felsic orthogneisses, 2 mafic granulites, 2 paragneisses and 2 charnockites, were chosen for U–Pb zircon dating, coupled with Lu–Hf isotopic analyses for magmatic zircon domains and whole-rock Sm–Nd isotopic analyses for felsic orthogneisses and mafic granulites. The sample localities are shown in Fig. 2 and the field occurrences of some dated samples are shown in Fig. 3. The location coordinates, mineral assemblages and age results are listed in Table 1.

Felsic orthogneisses (i.e., tonalitic–granitic gneisses) are the major component of the northern PCM. They generally display granoblastic textures with a weak to strong foliation. Almost all primary magmatic minerals and grain fabrics were obliterated during granulite facies metamorphism and deformation. Sample BL07-3 was collected from a thick (>50 m) layer of felsic orthogneiss at the southern edge of the Loewe Massif. It consists mainly of orthopyroxene, plagioclase, K-feldspar and quartz, with minor garnet, biotite and opaque oxides. Sample BL09-4 was taken from a thin (5–20 cm) felsic layer within mafic granulite on the western shore of Radok Lake (Fig.3a). This sample comprises hornblende, biotite, plagioclase, K-feldspar, quartz and opaque oxides, but lacks orthopyroxene. Samples BL10-1 and BL10-4 were taken from massive and banded felsic orthogneisses (Fig.3b–c), respectively,

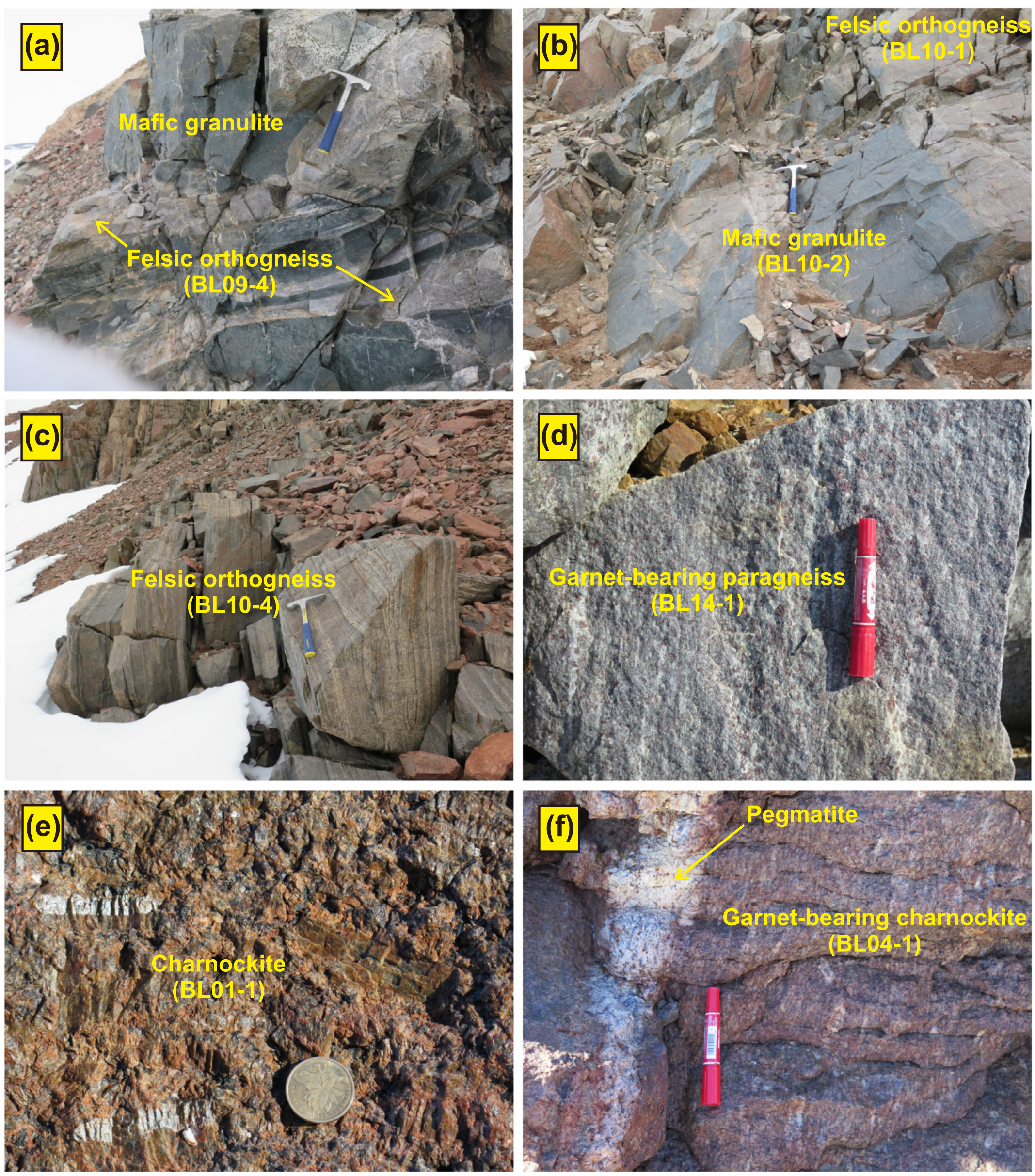


**Fig. 3.** Photographs showing the field occurrences of various rock types from the Beaver Lake area. (a) Felsic orthogneiss layers (Sample BL09-4) within mafic granulite from the western shore of Radok Lake. (b) A mafic granulite layer (dyke?) (sample BL10-2) within felsic orthogneiss (sample BL10-1) from the western shore of Radok Lake. (c) Banded felsic orthogneiss (sample BL10-4) from the western shore of Radok Lake. (d) Garnet-bearing paragneiss (sample BL14-1) from the southwestern shore of Radok Lake. (e) Massive charnockite (sample BL01-1) from the northern Loewe Massif. (f) Foliated charnockite (sample BL04-1) intruded by a pegmatite dyke from the northern Loewe Massif.

**Table 1**
Localities, lithology, mineral assemblages and age results of the studied samples from the Beaver Lake area.

| Sample | Location | Coordinates | Mineral assemblage | Ages (Ma) | | |
|---|---|---|---|---|---|---|
| | | | | Magmatism | Sedimentation | Metamorphism |
| *Felsic orthogneiss* | | | | | | |
| BL07-3 | Loewe Massif | S 70°38′24″<br>E 67°55′51″ | g, opx, bi, pl, ksp, q, op | 1070 ± 14 | | 921 ± 9 |
| BL09-4 | Radok Lake | S 70°50′34″<br>E 67°58′45″ | hb, bi, pl, ksp, q, op | 1150 ± 10 | | 915 ± 12 |
| BL10-1 | Radok Lake | S 70°51′14″<br>E 67°58′00″ | opx, cpx, hb, bi, pl, ksp, q, op | 1167 ± 18 | | 946 ± 13 |
| BL10-4 | Radok Lake | S 70°51′21″<br>E 67°57′52″ | opx, cpx, hb, bi, pl, ksp, q, op | 1096 ± 19 | | 922 ± 16 |
| *Mafic granulite* | | | | | | |
| BL10-2 | Radok Lake | S 70°51′14″<br>E 67°58′00″ | cpx, hb, bi, pl, op | | | 914 ± 5 |
| BL13-3 | Radok Lake | S 70°52′55″<br>E 67°54′55″ | opx, cpx, bi, pl, op | | | 914 ± 5 |
| *Paragneiss* | | | | | | |
| BL14-1 | Radok Lake | S 70°52′58″<br>E 67°55′00″ | g, bi, sill, cd, pl, ksp, q, sp, op | | <1200 | 930 ± 15 |
| BL15-3 | Else Platform | S 70°21′02″<br>E 68°52′14″ | g, bi, sill, cd, pl, ksp, q, sp, ru, op | | <1020 | 910 ± 92<br>520 ± 5 |
| *Charnockite* | | | | | | |
| BL01-1 | Loewe Massif | S 70°31′01″<br>E 68°00′23″ | opx, bi, pl, ksp, q, op | 949 ± 9 | | |
| BL04-1 | Loewe Massif | S 70°34′38″<br>E 67°57′42″ | g, opx, bi, pl, ksp, q, op | 1050 ± 11 | | 930 ± 9 |

bi, biotite; cd, cordierite; cpx, clinopyroxene; g, garnet; hb, hornblende; ksp, K-feldspar; op, opaque mineral; opx, orthopyroxene; pl, plagioclase; q, quartz; ru, rutile; sill, sillimanite; sp, spinel.

which dominate main outcrops on the western shore of Radok Lake. They have similar mineral assemblages of orthopyroxene + clinopyroxene + hornblende + biotite + plagioclase + K-feldspar + quartz + opaque oxides.

Mafic granulites are a volumetrically minor, but widespread constituent of the northern PCM. Most of them occur as pods, boudins, bands and layers within the felsic orthogneisses and paragneisses. Sample BL10-2 was collected from a 2 m wide discontinuous mafic layer (dyke?) hosted by felsic orthogneiss on the western shore of Radok Lake (see Fig.3b). It is composed of clinopyroxene, hornblende, biotite, plagioclase and opaque oxides. Sample BL13-3 was taken from a 5 m wide continuous mafic layer hosted by paragneiss on the southwestern shore of Radok Lake. This sample exhibits an equilibrium paragenesis of orthopyroxene + clinopyroxene + plagioclase + opaque oxides, along with minor biotite.

Paragneisses (i.e., metasedimentary rocks) are an important lithotype in the northern PCM. Well-preserved paragneisses are medium- to coarse-grained and commonly contain garnet porphyroblasts (Fig.3d). Much of the paragneiss has undergone extensive partial melting, leading to the formation of thickly layered leucogneisses and cm- to m-wide pegmatite boudins and dykes. Samples BL14-1 and BL15-3 were collected from the southwestern shore of Radok Lake and the Else Platform, respectively. The two samples contain similar mineral assemblages that include garnet + biotite + sillimanite + cordierite + plagioclase + K-feldspar + quartz + spinel + opaque oxides, except rutile also occurs in sample BL15-3.

Charnockites are voluminous and commonly form large batholiths in the northern PCM and on the Mawson Coast. Samples BL01-1 and BL04-1 were both taken from the northern Loewe Massif, but they have different field occurrences and show distinct petrographic characteristics. Sample BL01-1 is massive and unfoliated, with numerous large (up to 1–5 cm) feldspar phenocrysts that are randomly oriented or show only a weak preferred orientation (Fig.3e). The dominant minerals are orthopyroxene, biotite, plagioclase, K-feldspar and quartz, with minor opaque oxides. Sample BL04-1 is strongly foliated, with minor feldspar phenocrysts (<5 cm) that display a strong preferred orientation. The rock contains intrusive pegmatite dykes (1 cm to 1 m wide), within which the relics of fine-grained garnet- and orthopyroxene-bearing gneiss bands can be observed. The pegmatite dykes and associated gneiss bands are generally oriented parallel to the gneissosity of the charnockite (Fig.3f). This sample has mineral assemblage similar to sample BL01-1, but with the addition of minor garnet. Small-scale vermicular garnet coronas grew on the rims of large garnets, orthopyroxenes and opaque oxides, indicating metamorphic garnet growth.

### 3.2. Analytical procedures

U–Th–Pb isotopic analyses of magmatic and metamorphic zircons from metamorphic rocks and charnockites were carried out using a sensitive high-resolution ion microprobe (SHRIMP II) at the Beijing SHRIMP Centre, Chinese Academy of Geological Sciences, Beijing, China. Prior to analysis, zircon was extracted using conventional techniques, including crushing, sieving, heavy liquid separation and handpicking. The resulting zircon grains were then mounted in epoxy discs along with a TEMORA zircon standard and polished to expose the grain centers. Internal zircon structures were revealed by cathodoluminescence (CL) imaging. For the SHRIMP analyses, the instrumental conditions and data acquisition procedures followed Williams (1998), employing a 10 kV $O_2^-$ primary ion beam with a current of 4.5 nA. The spot diameter was set to 35 μm for samples BL10-1, BL10-2 and BL10-4, and to 25 μm for the remaining samples. Five scans through the mass stations were made for each age determination. Measured $^{206}Pb/^{238}U$ ratios were calibrated by analysis of the TEMORA reference zircon (416.75 ± 0.24 Ma; Black et al., 2003). Common Pb was corrected using measured $^{204}Pb$ values. Ages were calculated using the SQUID 1.03 (Ludwig, 2001) and ISOPLOT 3.23 (Ludwig, 2003) software programs. The age uncertainties for individual analyses are reported as one standard deviation (1σ), and the calculated weighted mean $^{206}Pb/^{238}U$ or $^{207}Pb/^{206}Pb$ ages are quoted at the 95% confidence level. The results of these analyses are listed in Table S1.

U–Th–Pb isotopic analyses of detrital zircons from the metasedimentary rocks were performed using laser–ablation inductively coupled plasma–mass spectrometry (LA–ICP–MS) at the State Key Laboratory of Geological Processes and Mineral Resources, China University of Geosciences, Wuhan, China. Detailed operating conditions for the laser ablation system and the analytical method employed are similar to those described by Hu et al. (2008). The zircon grains were mounted in an epoxy disc and polished to two-thirds of their original thickness. During the analyses, the output energy was set to 60 mJ, with a pulse repetition rate of 10 Hz and a 24 μm diameter laser spot size. For U, Th, and Pb analyses, $^{43}Ca$ calibration used the NIST610 reference glass and $^{29}Si$ as an internal standard, in combination with the working values recommended by Pearce et al. (1996). Isotopic ratios were calculated using ICPMSDataCal 8.0 (Liu et al., 2010), then corrected for both instrumental mass bias and depth-dependent elemental and isotopic fractionation using Harvard zircon 91500 ($^{206}Pb/^{238}U$ age = 1065.4 ± 0.6 Ma; Wiedenbeck et al., 1995) as an external standard. Ages were obtained using the software package ISOPLOT 3.23 (Ludwig, 2003). A common Pb correction was applied using ComPbCorr#3_17 (Andersen, 2002). As with the SHRIMP results, the age uncertainties presented for individual analyses are one standard deviation (1σ), and calculated weighted mean ages are quoted at the 95% (2σ) confidence level. The analytical data are presented in Tables S2.

Zircon Lu–Hf isotopic analyses were conducted using laser ablation–multicollector–inductively coupled plasma–mass spectrometry (LA–MC–ICP–MS) at the State Key Laboratory of Geological Processes and Mineral Resources, China University of Geosciences, Wuhan, China, following the procedure described by Hu et al. (2012). All data were acquired in single spot ablation mode using a spot size of 44 μm. Each measurement consisted of 20 s of background signal acquisition, followed by 50 s of ablation signal acquisition. In this study, we used the mass fractionation of Yb ($\beta_{Yb}$) obtained directly from the zircon samples in real-time. $^{179}Hf/^{177}Hf$ and $^{173}Yb/^{171}Yb$ ratios were then used, respectively, to calculate the mass bias of Hf ($\beta_{Hf}$) and Yb ($\beta_{Yb}$), which were in turn normalized to $^{179}Hf/^{177}Hf = 0.7325$ and $^{173}Yb/^{171}Yb = 1.132685$ (Fisher et al., 2014) using an exponential correction for mass bias. We corrected for interference of $^{176}Yb$ on $^{176}Hf$ by measuring the interference-free $^{173}Yb$ isotope signal and using $^{176}Yb/^{173}Yb = 0.79639$ (Fisher et al., 2014) as a baseline value in calculations of $^{176}Yb/^{177}Hf$. Similarly, the relatively minor interference of $^{176}Lu$ on $^{176}Hf$ was corrected by measuring the interference-free $^{175}Lu$ isotope signal and using the recommended ratio of $^{176}Lu/^{175}Lu = 0.02656$ (Blichert-Toft et al., 1997) to calculate $^{176}Lu/^{177}Hf$. In view of their similar physicochemical properties, we used the mass bias of Yb ($\beta_{Yb}$) to calculate the mass fractionation of Lu. Offline selection and integration of analytical signals and mass bias calibrations were performed using the ICPMSDataCal software package (Liu et al., 2010). We adopted a decay constant of $1.867 \times 10^{-11}$/year for $^{176}Lu$ (Söderlund et al., 2004) and presentday chondritic ratios of $^{176}Hf/^{177}Hf = 0.282785$ and $^{176}Lu/^{177}Hf = 0.0336$ (Bouvier et al., 2008) to calculate epsilon Hf values ($\varepsilon_{Hf}$). Single-stage Hf model ages ($T^{Hf}_{DM1}$) were calculated relative to the depleted mantle with a present-day $^{176}Hf/^{177}Hf$ ratio of 0.28325 and $^{176}Lu/^{177}Hf$ ratio of 0.0384 (Vervoort and Blichert-Toft, 1999). Two-stage Hf model ages ($T^{Hf}_{DM2}$) were calculated by assuming a mean $^{176}Lu/^{177}Hf$ value of 0.015 for the average continental crust (Griffin et al., 2002). The analytical and calculated results are shown in Table S3.

Nd isotopic analyses were performed at the Institute of Geology, Chinese Academy of Geological Sciences, Beijing, China. The analytical procedures are the same as reported by He et al. (2007). Prior to analysis, Sm and Nd were separated using the conventional ion exchange techniques, and their concentrations were determined using a Finnigan MAT 262 multi-collector mass spectrometer. Nd isotope compositions were acquired by a Nu Plasam HR MC–ICP-MS (Nu Instruments). Total procedural blanks are <100 pg for Sm and Nd, with Nd isotopic fractionation corrected to $^{146}Nd/^{144}Nd = 0.7219$. The within-run precision (2σ) for Nd analysis was estimated to be ±0.000011. During the period of data acquisition, the JMC $Nd_2O_3$ standard yielded $^{143}Nd/^{144}Nd = 0.511127 \pm 0.000010$ (2σ). Single-stage Nd depleted-mantle model ages ($T^{Nd}_{DM1}$) were calculated assuming a linear isotopic evolution of the depleted mantle reservoir from $\varepsilon_{Nd}(t) = 0$ at 4.56 Ga to +10 at the present. Two-stage Nd model ages ($T^{Nd}_{DM2}$) were obtained assuming that magmatic protoliths have the Sm/Nd ratio of the average continental crust (Keto and Jacobsen, 1987). The analytical and calculated results are presented in Table 2.

## 4. SHRIMP U–Pb zircon ages

SHRIMP U–Th–Pb isotopic analyses show different degrees of data dispersion for zircons from different samples. For zircons with complex internal structures from felsic orthogneisses, paragneisses and charnockites, some analytical data from both oscillatory-zoned and overgrowth domains are dispersed along a discordia trajectory due to partial lead loss or occasionally reverse discordance. In such a case, $^{207}Pb/^{206}Pb$ ages are more meaningful and were therefore used in the data interpretation. By contrast, for zircons with simple internal structures from mafic granulites, all analyses are highly clustered and nearly concordant, hence $^{206}Pb/^{208}U$ ages were used in the data interpretation.

### 4.1. Felsic orthogneisses

Zircons from sample BL07-3 are mostly long prismatic (100–250 μm) with aspect ratios of 2.0–4.0, although some grains have oval or irregular morphologies. In CL images, the majority of these zircons exhibit consistent core–rim variations that are characterized by oscillatory zoning in the cores and weak luminescence in the rims (Fig. 4a–b). A few grains have moderately luminescent outer overgrowths (Fig. 4c). Thirty U–Pb analyses were undertaken on 15 zircon cores, 14 rims and 1 outer overgrowth. Zircon cores

**Table 2**
Sm-Nd isotopic analyses for felsic orthogneisses and mafic granulites from the Beaver Lake area.

| Sample | Age (Ma) | Sm (ppm) | Nd (ppm) | $^{147}Sm/^{144}Nd$ | $^{143}Nd/^{144}Nd$ | ±2σ | $f_{Sm/Nd}$ | $\varepsilon_{Nd}(0)$ | $\varepsilon_{Nd}(T)$ | $T_{DM1}$ (Ga) | $T_{DM1}$ (Ga) |
|---|---|---|---|---|---|---|---|---|---|---|---|
| *Felsic orthogneiss* | | | | | | | | | | | |
| BL07-3 | 1070 | 9.044 | 45.374 | 0.1206 | 0.511917 | 0.000008 | −0.39 | −14.1 | −3.7 | 2.01 | 1.99 |
| BL09-4 | 1150 | 2.083 | 11.197 | 0.1125 | 0.511994 | 0.000005 | −0.43 | −12.6 | −0.2 | 1.74 | 1.77 |
| BL10-1 | 1167 | 4.951 | 24.668 | 0.1214 | 0.511989 | 0.000008 | −0.38 | −12.7 | −1.5 | 1.91 | 1.89 |
| BL10-4 | 1096 | 9.523 | 49.394 | 0.1166 | 0.511997 | 0.000005 | −0.41 | −12.5 | −1.3 | 1.80 | 1.82 |
| *Mafic granulites* | | | | | | | | | | | |
| BL10-2 | 1167 | 6.321 | 23.296 | 0.1641 | 0.512451 | 0.000009 | −0.17 | −3.6 | 1.2 | 2.14 | 1.67 |
| BL13-3 | 1167 | 3.952 | 13.241 | 0.1805 | 0.51256 | 0.000012 | −0.08 | −1.5 | 0.9 | 2.69 | 1.70 |

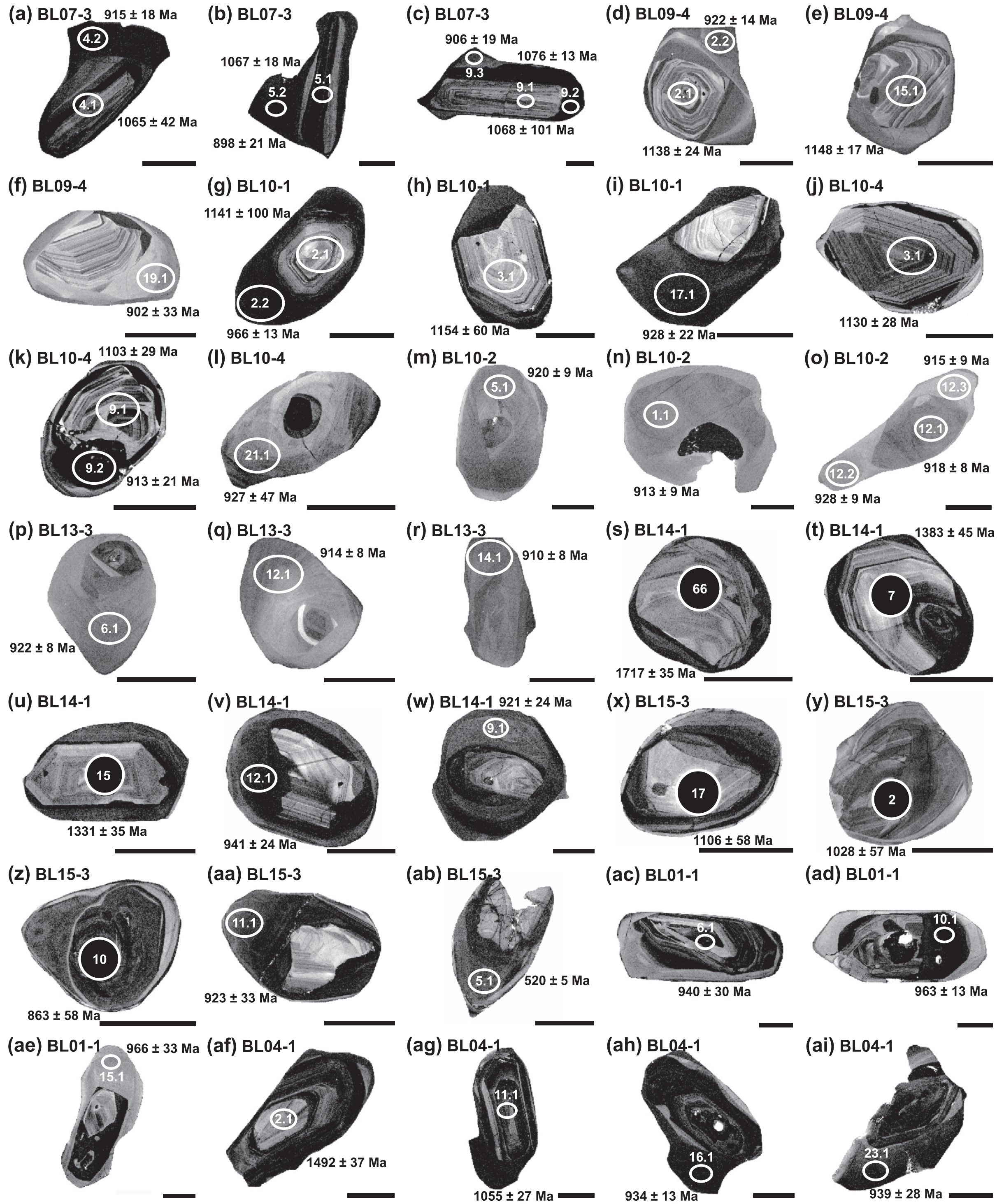


**Fig. 4.** Cathodoluminescence (CL) images of representative zircons from various rock types in the Beaver Lake area. (a–b) Zircon from sample BL07-3 showing an oscillatory-zoned core and a weakly luminescent rim. (c) Zircon from sample BL07-3 showing an oscillatory-zoned core, a weakly luminescent rim and a moderately luminescent outer rim. (d–f) Zircon from sample BL09-4 showing an oscillatory-zoned core and a strongly luminescent rim. (g–i) Zircon from sample BL10-1 showing an oscillatory-zoned core and a weakly luminescent rim. (j–k) Zircon from sample BL10-4 showing an oscillatory-zoned core, a weakly luminescent mantle and a strongly luminescent narrow rim. (l) Zircon from sample BL10-4 showing a small CL-dark relict core and a strongly luminescent rim with fir-tree zoning. (m) Zircon from sample BL10-2 showing sector zoning and containing a CL-dark relict core. (n-o) Zircon from sample BL10-2 showing an weakly luminescent core and a strongly luminescent rim with sector zoning. (p–q) Zircon from sample BL13-3 showing a small CL-dark relict core and a strongly luminescent overgrowth with sector zoning. (r) Zircon from sample BL13-3 showing weak luminescence with fir-tree zoning. (s–w) Zircon from sample BL14-1 showing an oscillatory-zoned core and a weakly luminescent rim. (x–aa) Zircon from sample BL15-3 showing an oscillatory-zoned core and a moderately or weakly luminescent rim. (ab) Zircon from sample BL15-3 showing a CL-bright homogeneous core and a moderately luminescent rim with sector zoning. (ac–ae) Zircon from sample BL01-1 showing an oscillatory-zoned core, a weakly luminescent mantle and a strongly luminescent rim. (af) Zircon from sample BL04-1 showing a CL-bright oscillatory-zoned core, a CL-dark oscillatory-zoned mantle and a thin, weakly luminescent rim. (ag–ai) Zircon from sample BL04-1 showing an oscillatory-zoned core and a discontinuous, weakly luminescent overgrowth rim. Ages are given with errors of 1σ. Scale bars are 50 μm.

have U concentrations of 292–1332 ppm and Th concentrations of 54–505 ppm, with Th/U ratios of 0.07–0.51. Of these, 13 analyses yield $^{207}Pb/^{206}Pb$ ages ranging from 1140 ± 44 to 1054 ± 23 Ma, defining a weighted mean $^{207}Pb/^{206}Pb$ age of 1070 ± 14 Ma (MSWD = 0.44) that is within error of the upper intercept age of 1086 ± 45 Ma (MSWD = 0.31) (Fig. 5a). Two other analyses produce younger $^{207}Pb/^{206}Pb$ ages of 970 ± 98 Ma (spot 3.1) and 913 ± 50 Ma (spot 15.1). Zircon rims and outer overgrowth have U concentrations of 675–1463 ppm and Th concentrations of 46–264 ppm, with Th/U ratios of 0.02–0.35. Except for one analysis that yield an old $^{207}Pb/^{206}Pb$ age of 1076 ± 13 Ma age (spot 9.2), the remaining 14 analyses have similar $^{207}Pb/^{206}Pb$ ages that define a weighted mean age of 921 ± 9 Ma (MSWD = 0.71) and an upper intercept age of 922 ± 11 Ma (MSWD = 0.68).

Zircons from sample BL09-4 are oval to short prismatic and 50–160 µm long. They all have oscillatory-zoned cores and strongly luminescent overgrowth rims (Fig. 4d–f). Thirty spot analyses were performed on 15 zircon cores and 15 rims. The zircon cores contain U and Th abundances of 297–539 ppm and 166–418 ppm, respectively, with Th/U ratios of 0.49–0.97. They yield a weighted mean $^{207}Pb/^{206}Pb$ age of 1150 ± 10 Ma (MSWD = 0.64), which is within error of the upper intercept age of 1147 ± 16 Ma (MSWD = 0.67) (Fig. 5b). The zircon rims contain 173–898 ppm U and 108–460 ppm Th, with Th/U ratios of 0.32–0.74. They produce a weighted mean $^{207}Pb/^{206}Pb$ age of 915 ± 12 Ma (MSWD = 0.67) and an upper intercept age of 912 ± 17 Ma (MSWD = 0.71).

Zircons from sample BL10-1 show short to medium prismatic morphologies with lengths of 60–170 µm. The majority of these zircons have oscillatory-zoned cores and weakly luminescent rims (Fig. 4g–i). Thirty analyses were conducted on 15 zircon cores and 15 rims. The zircon cores have U contents of 153–440 ppm and Th contents of 64–299 ppm, with Th/U ratios of 0.41–0.70. They yield the same (within error) weighted mean $^{207}Pb/^{206}Pb$ and upper intercept ages of 1167 ± 18 Ma (MSWD = 0.60) and 1166 ± 29 Ma (MSWD = 0.64), respectively (Fig. 5c). The zircon rims have U contents of 505–2101 ppm and Th contents of 200–511 ppm, with Th/U ratios of 0.10–0.79. Except for outlier data points 23.1 (877 ± 21 Ma) and 26.1 (1011 ± 13 Ma), the remaining 13 analyses produce a weighted mean $^{207}Pb/^{206}Pb$ age of 946 ± 13 Ma (MSWD = 1.9) that is within error of the upper intercept age of 951 ± 24 Ma (MSWD = 1.6).

Zircons from sample BL10-4 are short to medium prismatic with prism lengths varying from 60 to 280 µm. Well-preserved zircon grains commonly show complex core–mantle–rim features that are characterized by oscillatory zoning in the cores, weak luminescence in the mantles and strong luminescence in the rims (Fig. 4j–k). In some cases, the oscillatory-zoned cores are absent (Fig. 4l). Thirty-three zircon analyses were carried out on 15 cores, 6 mantles and 12 rims. The zircon cores have variable U (171–1345 ppm) and Th (83–1382 ppm) concentrations, with Th/U ratios of 0.39–1.06. Barring spot 1.1 with an age of 1162 ± 17 Ma and spot 7.1 with an age of 1011 ± 29 Ma, the other 13 analyses yield a weighted mean $^{207}Pb/^{206}Pb$ age of 1096 ± 19 Ma (MSWD = 0.70), which is within error of the upper intercept age of 1117 ± 50 Ma (MSWD = 0.46) (Fig. 5d). In general, the zircon mantles have higher U and Th concentrations (U = 426–2449 ppm; Th = 144–338 ppm; Th/U = 0.06–0.50) than the zircon rims (U = 119–629 ppm; Th = 39–237 ppm; Th/U = 0.30–0.47).

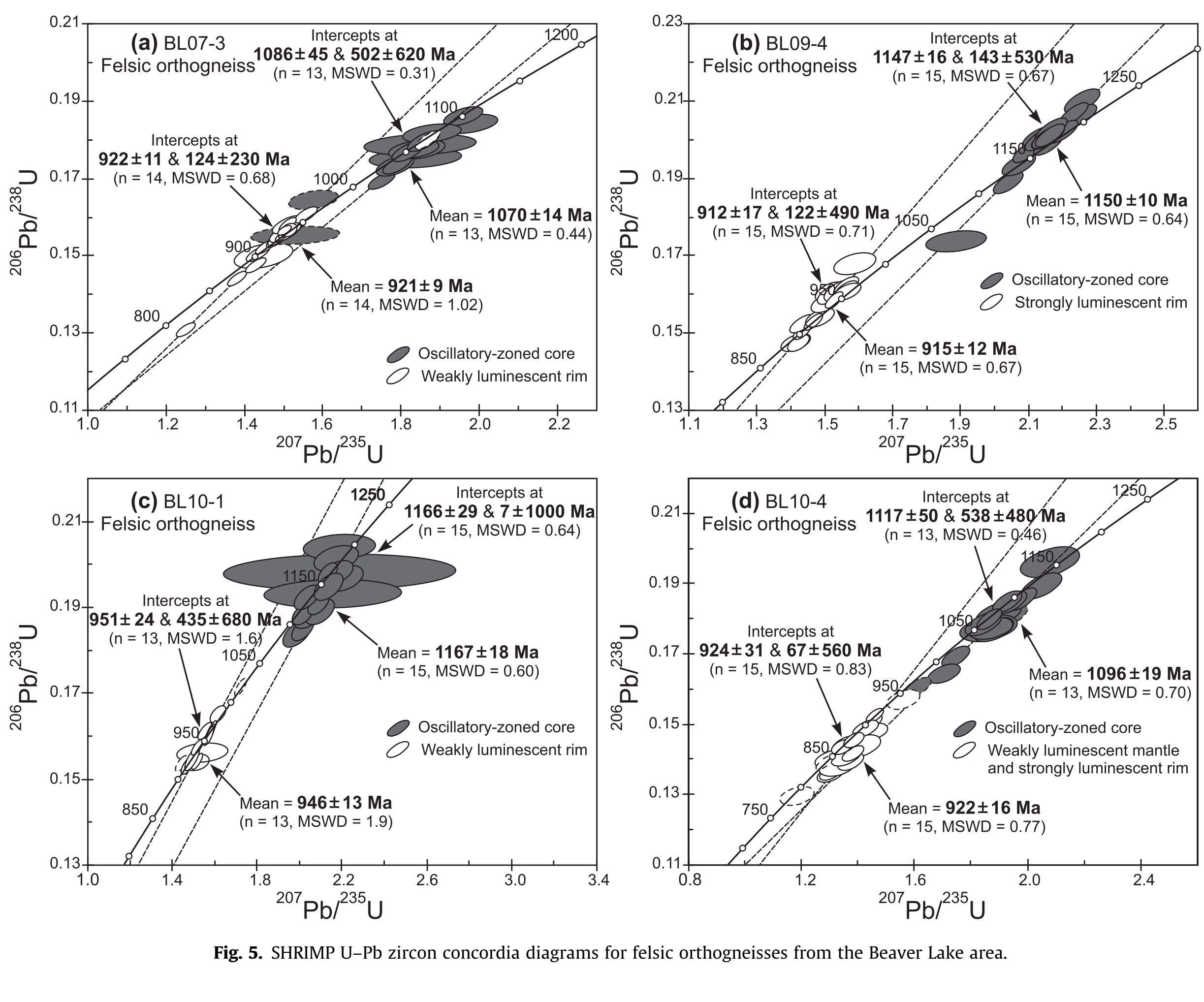


**Fig. 5.** SHRIMP U–Pb zircon concordia diagrams for felsic orthogneisses from the Beaver Lake area.

However, the $^{207}Pb/^{206}Pb$ ages of the mantles and rims are very similar. Excluding data points 18.2 (820 ± 66 Ma), 27.1 (835 ± 23 Ma) and 26.1 (990 ± 46 Ma), the remaining 15 analyses produce a weighted mean age of 922 ± 16 Ma (MSWD = 0.77) and an upper intercept age of 924 ± 31 Ma (MSWD = 0.83).

### 4.2. Mafic granulites

Zircons from sample BL10-2 are oval to spherical in shape with grain sizes of 80–200 μm. Most of them show weak luminescence and sector zoning, with or without a thin, irregular and strongly luminescent rim (Fig. 4m–o). Some grains have CL-dark relict cores (see Fig. 4m) that are too small to be analyzed. Fifteen zircon analyses were undertaken on 12 weakly luminescent domains and 3 strongly luminescent rims. The weakly luminescent domains have relatively high U and Th abundances of 194–491 ppm and 55–128 ppm, respectively, and Th/U ratios of 0.27–0.36. The strongly luminescent rims have lower U and Th abundances of 147–206 ppm and 43–65 ppm, respectively, and Th/U ratios of 0.30–0.33. U–Pb analyses on these two domains yield similar $^{206}Pb/^{238}U$ ages, with a weighted mean $^{206}Pb/^{238}U$ age of 914 ± 5 Ma (MSWD = 1.10; excluding data point 6.1 which produce a $^{206}Pb/^{238}U$ age of 885 ± 5 Ma) (Fig. 6a).

Zircons from sample BL 13–3 are oval to spherical with diameters of 40–120 μm. Most grains exhibit strong luminescence and sector or fir-tree zoning, with or without a small CL-dark relict core (Fig. 4p–q). Some of them have weakly luminescent rims (Fig. 4r). Fifteen zircon analyses were undertaken on 12 strongly luminescent domains and 3 weakly luminescent rims. The strongly luminescent domains have relatively low U (322–555 ppm) and Th (75–139 ppm) contents, with Th/U ratios of 0.24–0.28, whereas the weakly luminescent rims have higher U (624–823 ppm) and Th (155–207 ppm) contents, with Th/U ratios of 0.20–0.28. Both domains yield $^{206}Pb/^{238}U$ ages clustered between 928 ± 7 and 899 ± 7 Ma, with a weighted mean age of 914 ± 5 Ma (MSWD = 1.2) (Fig. 6b).

### 4.3. Paragneisses

Zircons from sample BL14-1 are oval to short prismatic with lengths of 40–220 μm. Almost all zircons exhibit core–rim structures that are defined by oscillatory zoning in the cores and weak luminescence in the rims (Fig. 4s–w). In some cases, the oscillatory bands in the cores are thickened and blurred. Fifteen spot analyses on the weakly luminescent rims show variable U concentrations of 445–1360 ppm and Th concentrations of 8–238 ppm, with Th/U ratios of 0.01–0.33. Five discordant analyses yield $^{207}Pb/^{206}Pb$ ages ranging from 1818 ± 19 to 1199 ± 17 Ma, and 10 near-concordant analyses produce younger ages with a weighted mean $^{207}Pb/^{206}Pb$ age of 930 ± 15 Ma (MSWD = 1.4) (Fig. 7a).

Zircons from sample BL15-3 are ovoid to short prismatic and 40–200 μm long. All of these zircons have oscillatory-zoned cores

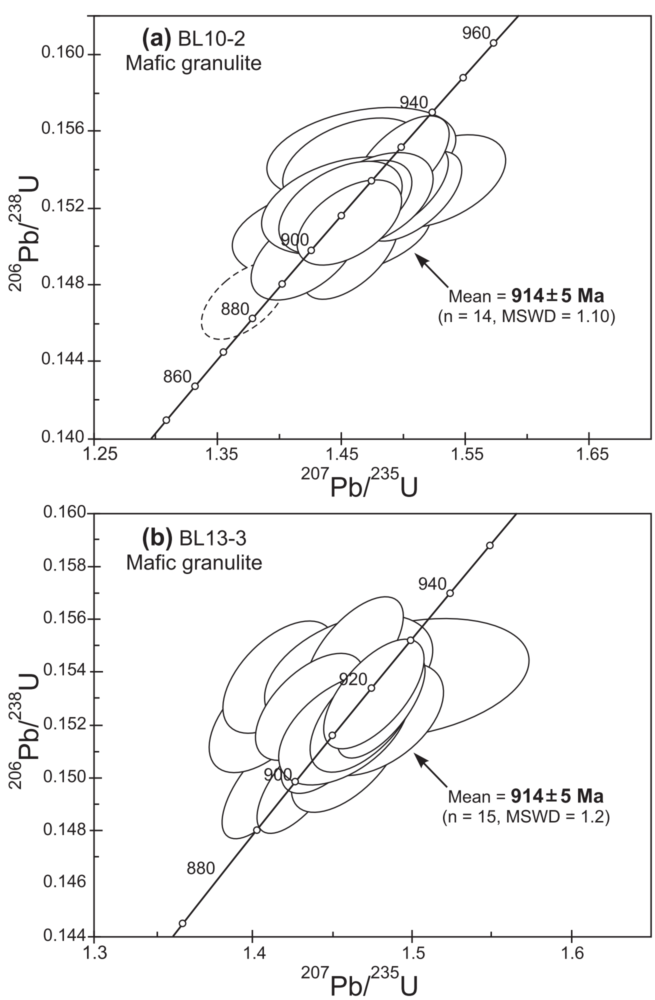


**Fig. 6.** SHRIMP U–Pb zircon concordia diagrams for mafic granulites from the Beaver Lake area.

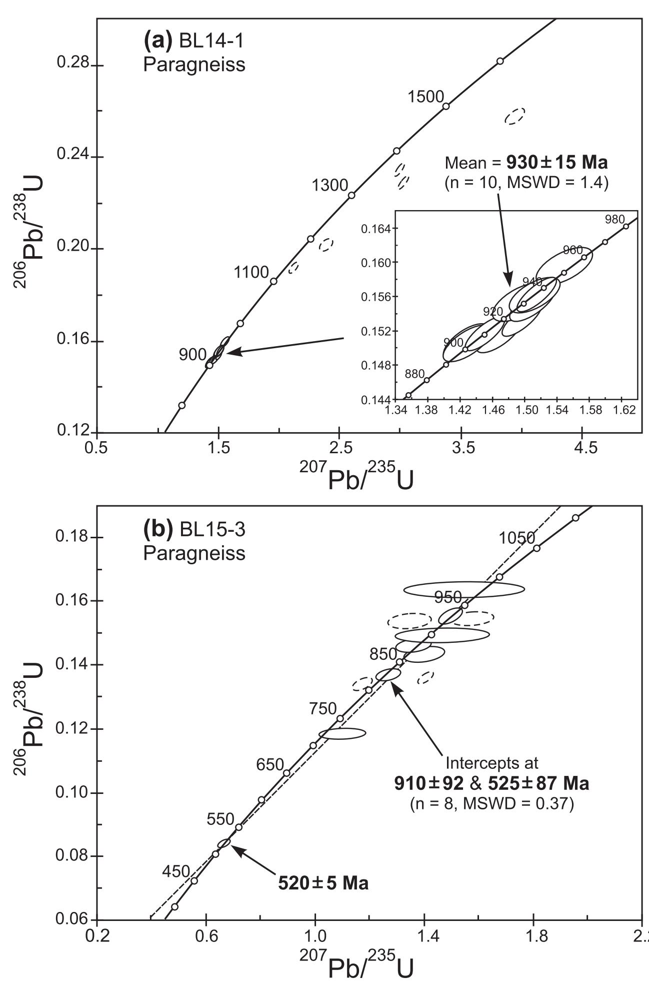


**Fig. 7.** SHRIMP U–Pb zircon concordia diagrams for paragneisses from the Beaver Lake area.

and moderately or weakly luminescent rims (Fig. 4x–ab). However, the oscillatory bands in many cores have been thickened, blurred, and even entirely homogenized (see Fig. 4y, z, ab). Twelve spot analyses on the moderately luminescent rims show U abundances of 154–962 ppm and Th abundances of 48–291 ppm, with variable Th/U ratios of 0.06–1.51. With the exception of 4 discordant spots, the remaining 8 analyses plot on or near a discordia, defining upper and lower intercept ages of 910 ± 92 Ma and 525 ± 87 Ma, respectively (MSWD = 0.37) (Fig. 7b). Note that spot 5.1 yields the youngest $^{206}Pb/^{238}U$ age of 520 ± 5 Ma in the sample set.

### 4.4. Charnockites

Zircons from sample BL01-1 are long prismatic with lengths of 130–380 μm and aspect ratios of 2.0–4.0. Well-preserved zircon grains display internal structures with oscillatory-zoned cores, weakly luminescent mantles and strongly luminescent rims (Fig. 4ac–ae). Twenty-seven analyses were performed on 9 zircon cores, 6 mantles and 12 rims. These different zircon domains have distinct U and Th contents and Th/U ratios, with U = 171–719 ppm, Th = 141–395 ppm and Th/U = 0.42–1.41 for the cores; U = 664–1554 ppm, Th = 176–664 ppm and Th/U = 0.16–0.79 for the mantles; and U = 89–255 ppm, Th = 25–69 ppm and Th/U = 0.27–0.32 for the rims. However, apart from 2 rim analyses with $^{207}Pb/^{206}Pb$ ages of 872 ± 37 Ma (spot 24.1) and 803 ± 53 Ma (spot 25.1), the remaining 25 analyses of the three domains yield similar $^{207}Pb/^{206}Pb$ ages with a weighted mean of 949 ± 9 Ma (MSWD = 0.70), which is within error of the upper intercept age of 946 ± 12 Ma (MSWD = 0.74) (Fig. 8a).

Zircons from sample BL04-1 have long prismatic forms with prism lengths of 100–320 μm and aspect ratios of 2.0–5.0. Most of these zircons have oscillatory-zoned cores and discontinuous, weakly luminescent overgrowth rims (Fig. 4af–ai). Some grains contain an oscillatory-zoned inner core (see Fig. 4af). Twenty-seven spot analyses were conducted on 15 zircon cores and 12 rims. The zircon cores contain variable U (128–1339 ppm) and Th (24–371 ppm) concentrations with Th/U ratios of 0.02–0.69. Among these analyses, 3 spots on inner cores yield older $^{207}Pb/^{206}Pb$ ages between 1492 ± 37 and 1243 ± 29 Ma (not shown in Fig. 8b) and 3 spots yield younger $^{207}Pb/^{206}Pb$ ages from 981 ± 24 Ma to 941 ± 36 Ma. The remaining 9 analyses produce similar $^{207}Pb/^{206}Pb$ ages that define a weighted mean age of 1050 ± 11 Ma (MSWD = 0.88) and an upper intercept age of 1043 ± 21 Ma (MSWD = 0.75) (see Fig. 8b). The zircon rims contain 505–1100 ppm U and 7–219 ppm Th, with Th/U ratios of 0.04–0.45. They yield a weighted mean $^{207}Pb/^{206}Pb$ age of 930 ± 9 Ma (MSWD = 0.97) that is within error of the upper intercept age of 930 ± 8 Ma (MSWD = 1.02).

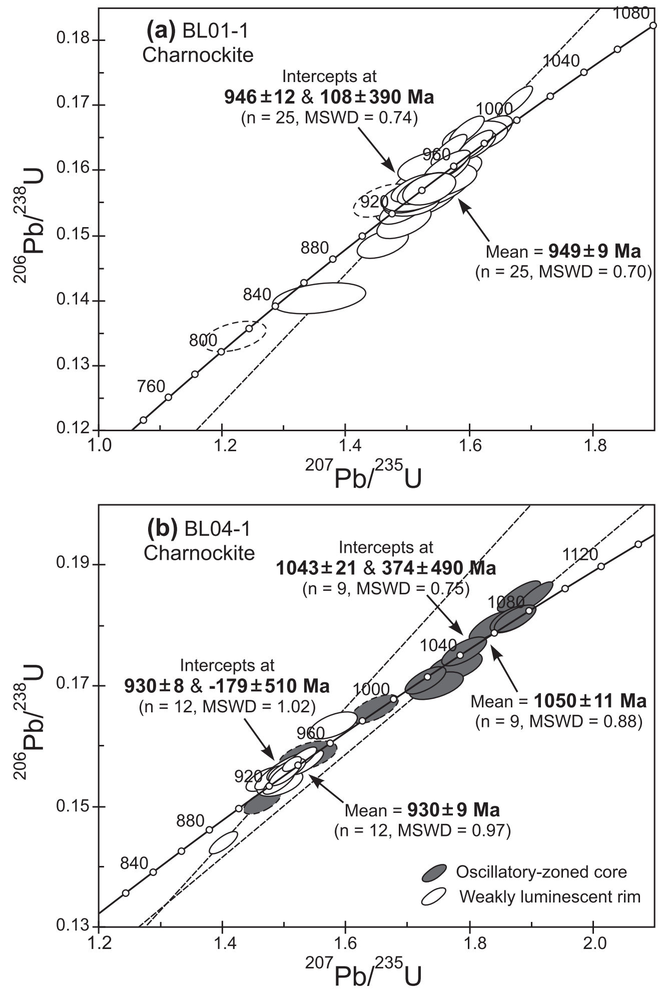


**Fig. 8.** SHRIMP U–Pb zircon concordia diagrams for charnockites from the Beaver Lake area.

## 5. LA–ICP–MS U–Pb zircon ages

LA–ICP–MS U–Th–Pb isotopic analyses were only carried out on the oscillatory-zoned cores of detrital zircons (except for one with sector zoning) from paragneiss samples BL14-1 and BL15-3. To obtain statistical significance for the provenance study, 120 randomly selected detrital zircon grains with well-preserved cores were dated for each sample. Taking into account the zircon overgrowth rims were determined to be ca. 930–910 Ma using SHRIMP method, $^{207}Pb/^{206}Pb$ ages were used in the data interpretation for all the core analyses. To avoid analytical bias due to lead loss or common lead contamination, zircons with U–Pb age concordance less than 90% were rejected during the construction of the age probability density diagrams (Fig. 9).

One hundred and twenty spot analyses on 120 oscillatory-zoned zircon cores from sample BL14-1 yield 119 near-concordant ages (≥90% concordance), ranging from 2128 ± 48 to 863 ± 47 Ma. A major age population occurs at ca. 1480–1140 Ma (*n* = 76, peak at ca. 1380 Ma), along with three subordinate age populations at ca. 2130–1850 Ma (*n* = 7, peak at ca. 2010 Ma), ca. 1800–1600 Ma (*n* = 19, peak at ca. 1700 Ma) and ca. 1010–860 Ma (*n* = 9, peak at ca. 920 Ma) (Fig. 9a). In the major age population, the 12 youngest dates from 1229 ± 43 to 1144 ± 44 Ma that are essentially within error of one another yield a weighted mean $^{207}Pb/^{206}Pb$ age of 1199 ± 29 Ma (MSWD = 0.28).

The age data obtained for 119 oscillatory-zoned zircon cores and 1 sector-zoned core from sample BL15-3 show an age spectrum different from that of sample BL14-1. Among them, 99 near-concordant zircon analyses yield $^{207}Pb/^{206}Pb$ ages ranging from 1665 ± 42 to 643 ± 94 Ma, with a major age population at ca. 1180–830 Ma (*n* = 87, peak at ca. 1020 Ma) and a subordinate age populations at ca. 1370–1230 Ma (*n* = 9, peak at ca. 1250 Ma) (Fig.9b). The youngest $^{206}Pb/^{238}U$ age of 531 ± 13 Ma is resulted from the analysis of the single sector-zoned zircon grain.

## 6. Zircon Lu–Hf isotopes

Lu–Hf isotopic analyses were performed on 15 oscillatory-zoned zircon cores for each of the 4 felsic orthogneiss samples. Zircons from 3 samples yield positive initial $\varepsilon_{Hf}$ values [$\varepsilon_{Hf}(t)$] and uniform two-stage Hf model ages ($T_{DM2}^{Hf}$). The $\varepsilon_{Hf}(t)$ values and corresponding $T_{DM2}^{Hf}$ ages are, respectively,+2.4 to +4.7 (average

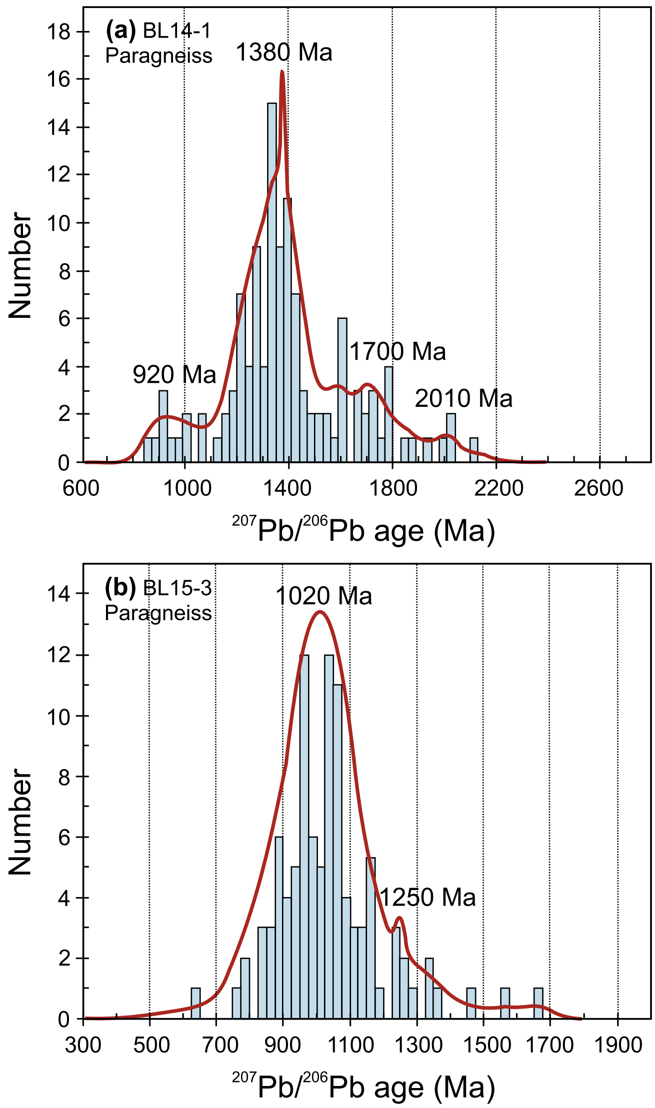


**Fig. 9.** Cumulative probability histograms of $^{207}Pb/^{206}Pb$ ages for near-concordant detrital zircons from paragneisses from the Beaver Lake area.

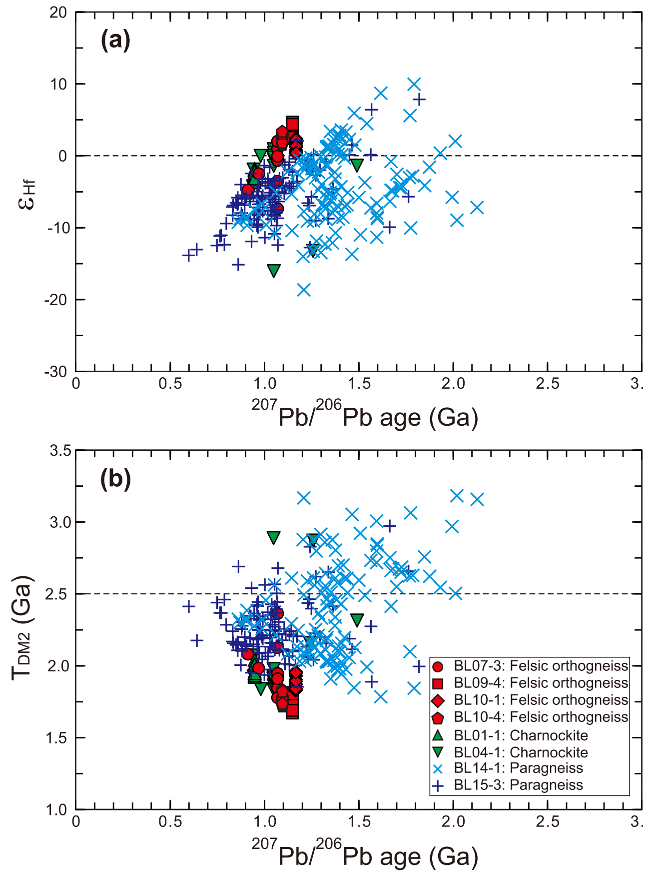


**Fig. 10.** Diagrams illustrating Hf isotopic compositions versus $^{207}Pb/^{206}Pb$ ages for magmatic zircons from felsic orthogneisses, charnockites and paragneisses from the Beaver Lake area. (a) Initial Hf ratios versus $^{207}Pb/^{206}Pb$ ages. (b) Hf model ages versus $^{207}Pb/^{206}Pb$ ages.

+3.6) and 1.81–1.67 Ga (average 1.74 Ga) for sample BL09-4, +0.3 to +2.4 (average +1.4) and 1.96–1.83 Ga (average 1.89 Ga) for sample BL10-1, and +1.5 to +3.3 (average +2.5) and 1.83–1.72 Ga (average 1.76 Ga) for sample BL10-4 (Fig. 10). In contrast, zircons from sample BL07-3 display slightly more variable Lu–Hf isotopic compositions. Eleven analyses yield $\varepsilon_{Hf}(t)$ values from −0.7 to +2.0 (average −0.1), with $T_{DM2}^{Hf}$ ages of 1.94–1.78 Ga (average 1.91 Ga). The remaining 4 data points have more negative $\varepsilon_{Hf}(t)$ values (−7.4 to −2.5) and older $T_{DM2}^{Hf}$ ages (2.36–1.98 Ga).

Nine oscillatory-zoned zircon cores from charnockite sample BL01-1 yield homogeneous $\varepsilon_{Hf}(t)$ values between −3.7 to −1.8 (average −2.6), with $T_{DM2}^{Hf}$ ages from 2.03 to 1.92 Ga (average 1.97 Ga). In another charnockite sample BL04-1, the majority of the oscillatory-zoned zircon cores (10 spots) produce $\varepsilon_{Hf}(t)$ values clustered between −1.9 and +0.9 (average −0.4), with corresponding $T_{DM2}^{Hf}$ ages of 1.98–1.83 Ga (average 1.90 Ga), whereas 5 other spots, including 3 zircon cores with older $^{207}Pb/^{206}Pb$ ages (1492–1243 Ma), show negative $\varepsilon_{Hf}(t)$ values varying from −16.1 to −1.4 and old $T_{DM2}^{Hf}$ ages from 2.89 to 2.07 Ga.

The Lu–Hf isotopic compositions for the oscillatory-zoned cores of the detrital zircons from paragneiss samples BL14-1 and BL15-3 are somewhat different one another, and no better correlations were observed between the ages and Hf isotopic compositions of zircons from both samples (Figs. 10–11). The majority of zircons from sample BL14-1 show a broad range of $\varepsilon_{Hf}(t)$ values from −12 to +4, with several exceptions with very low and very high values (roughly from −19 to −13 and +6 to +10, respectively) (Fig. 11a). Excluding these exceptions, the $T_{DM2}^{Hf}$ ages can be grouped into two populations at ca. 3.0–2.4 Ga and ca. 2.3–1.9 Ga (Fig. 11b). In contrast, the $\varepsilon_{Hf}(t)$ values of zircons from sample BL15-3 are mainly concentrated between −10 to 0, with a small number being scattered at −15 to −11 and +2 to +8 (Fig. 11c). Their $T_{DM2}^{Hf}$ ages are mainly clustered between 2.6 and 1.9 Ga, although a number of ages plot beyond this range (Fig. 11d).

## 7. Whole-rock Sm–Nd isotopes

Felsic orthogneisses display uniform and evolved Sm–Nd isotopic signatures. They have small ranges of initial $\varepsilon_{Nd}$ values [$\varepsilon_{Nd}(t)$] from −3.7 to −0.2 and two-stage Nd depleted mantle model ages ($T_{DM2}^{Nd}$) of 1.99–1.77 Ga. Mafic granulites yield positive $\varepsilon_{Nd}(t)$ values from +0.9 to +1.2, with $T_{DM2}^{Nd}$ ages of 1.70–1.67 Ga.

## 8. Discussion

### *8.1. Protolith ages and sources of metaigneous rocks*

The protolith ages of mafic granulites and felsic orthogneisses from the northern PCM are poorly constrained. The earliest date in this area comes from an imprecise whole-rock Rb–Sr isochron

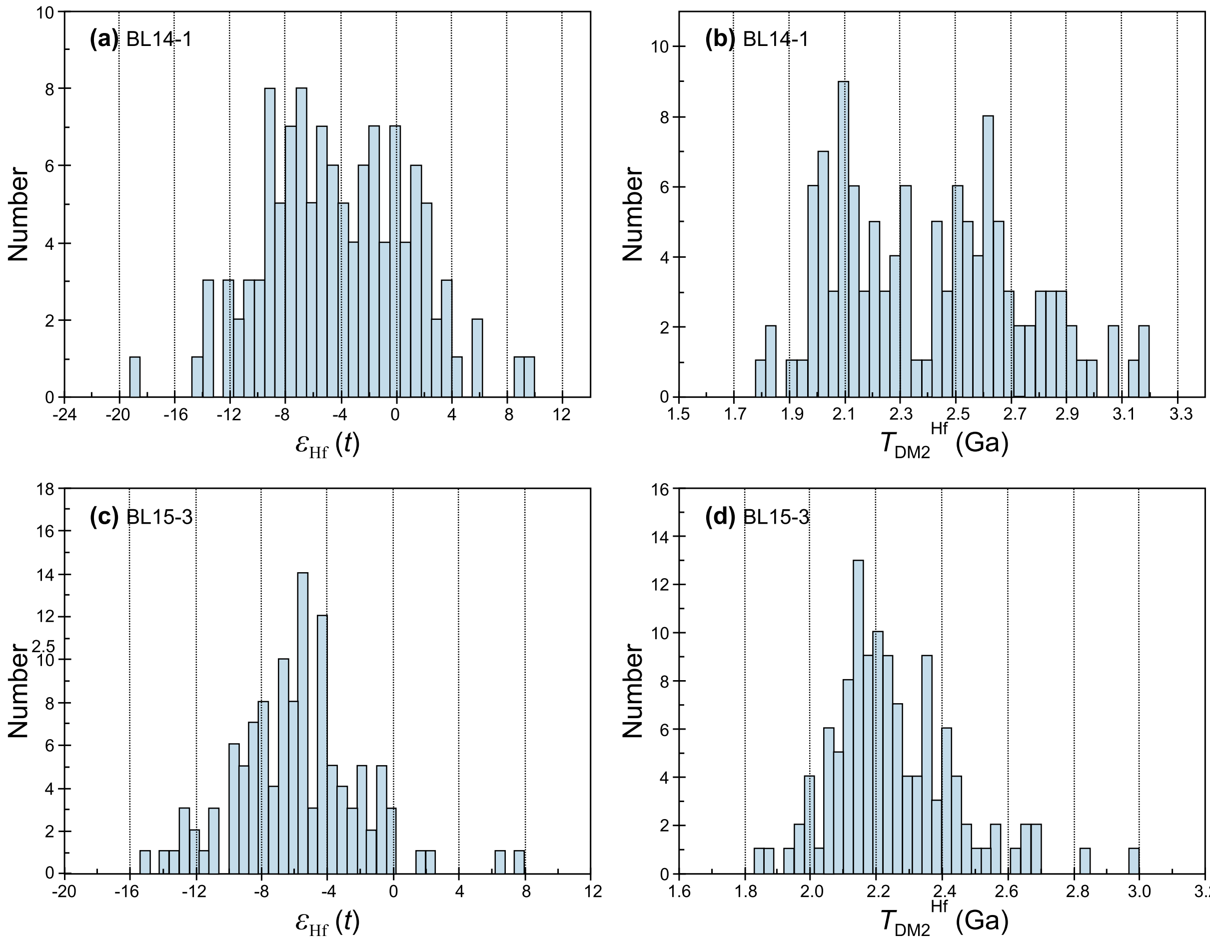


**Fig. 11.** Cumulative probability histograms of the initial Hf ratios (a and c) and Hf model ages (b and d) for detrital zircons from paragneisses from the Beaver Lake area.

age of 1033 ± 85 Ma for felsic gneiss from the Martin Massif (Tingey, 1982, 1991). The subsequent U–Pb dating of magmatic zircons also gave relatively young ages of 1017 ± 31 Ma (leucosome from Radok Lake; Boger et al., 2000), 1071 ± 23 Ma (gneissic granite from the McLeod Massif; Kamenev et al., 2009), and 1044 ± 10 Ma (felsic orthogneiss from the Porthos Range; Mikhalsky and Sheraton, 2011) (Table 3). Our new SHRIMP U–Pb isotopic analyses of zircon cores from felsic orthogneisses from the Beaver Lake area yield four precise ages: 1167 ± 18 Ma for sample BL10-1, 1150 ± 10 Ma for sample BL09-4, 1096 ± 19 Ma for sample BL10-4, and 1070 ± 14 Ma for sample BL07-3. The analyzed zircon cores show oscillatory zoning and have Th/U ratios mostly more than 0.30, suggesting that these ages represent the ages of the felsic orthogneiss protoliths. In fact, three similar, unpublished U–Pb zircon ages of 1147 ± 16 (metagabbro from the McLeod Massif), 1045 ± 2 and 1064 ± 2 Ma (felsic orthogneiss from the Aramis Range) have been reported by Mikhalsky et al. (2013). This seems to suggest that pre-metamorphic magmatic activity in the northern PCM occurred mainly at ca. 1170–1020 Ma. However, an older age of 1324 ± 13 Ma was also obtained for a felsic orthogneiss from Mount Lanyon, the southernmost outcrop of the Rayner Complex (Mikhalsky et al., 2013; unpublished data). This highlights an inconsistency in metaigneous protolith ages in the northern PCM, and suggests that further investigation is required.

Lu–Hf isotopic analyses indicate that most magmatic zircons from the felsic orthogneisses have homogeneous, less evolved Hf isotopic compositions, with $\varepsilon_{\mathrm{Hf}}(t)$ values from −0.1 to +3.6 and corresponding $T_{\mathrm{DM2}}^{\mathrm{Hf}}$ ages of 1.91–1.74 Ga. This suggests that the felsic magmas were derived from ancient crustal rocks that were extracted from mantle during the Paleoproterozoic. A few data points from sample BL07-3 show relatively low $\varepsilon_{\mathrm{Hf}}(t)$ values (−7.4 to −2.5) and older $T_{\mathrm{DM2}}^{\mathrm{Hf}}$ ages (2.36–1.98 Ga), implying some assimilation of the country rocks during the generation of felsic magma generation. It is interesting to note that the $T_{\mathrm{DM2}}^{\mathrm{Hf}}$ ages of zircons are in agreement with the whole-rock $T_{\mathrm{DM2}}^{\mathrm{Nd}}$ ages (1.99–1.77 Ga) obtained for the felsic orthogneisses, although $\varepsilon_{\mathrm{Nd}}(t)$ values (−3.7 to −0.2) of the rocks are lower than $\varepsilon_{\mathrm{Hf}}(t)$ values of zircons. Over the much of the northern PCM, the $T_{\mathrm{DM}}^{\mathrm{Nd}}$ ages range from 2.38 to 1.60 Ga (Mikhalsky et al., 2001, 2006a; Mikhalsky, 2008; Mikhalsky and Sheraton, 2011). Therefore, both zircon Hf and whole-rock Nd isotopic compositions indicate significant Paleoproterozoic crustal growth in the northern PCM. Furthermore, major and trace element geochemistry demonstrate that these felsic igneous rocks may have formed in an active continental margin or continental arc setting during the late Mesoproterozoic (Munksgaard et al., 1992; Sheraton et al., 1996; Stephenson, 2000; Mikhalsky et al., 1996, 2001).

### 8.2. Depositional ages and provenance of metasedimentary rocks

Detrital zircons from paragneiss samples BL14-1 and BL15-1 exhibit slightly different age spectra. Zircons from sample BL14-1 collected from Radok Lake have four age populations at ca. 2130–1850, ca. 1800–1600, ca. 1480–1140 and ca. 1010–860 Ma. The youngest population overlaps with the metamorphic age yielded by zircon overgrowth rims from the same sample and may therefore have resulted from solid-state recrystallization during metamorphism as indicated by the thickened and blurred

**Table 3**
Summary of published zircon and monazite U–Pb age data of rocks from the northern Prince Charles Mountains and adjacent Mawson Coast.

| Location | Sample | Rock type | Dating method | Magmatic age (Ma) | Metamorphic age (Ma) | Reference |
|---|---|---|---|---|---|---|
| *Northern Prince Charles Mountains* | | | | | | |
| Else Platform | 625 | felsic gneiss | ID-TIMS zircon | | 1000 + 14/−11 | Manton et al., 1992 |
| | 669A | granite | ID-TIMS zircon | 524 + 6/−112 | | Manton et al., 1992 |
| | 670A | granite | ID-TIMS zircon | 565 + 25/−12 | | Manton et al., 1992 |
| Jetty Peninsula | 675 | gneissic leucogranite | ID-TIMS zircon | 940 + 24/−17 | | Manton et al., 1992 |
| | 609E | pegmatite | ID-TIMS zircon | ca. 500 | | Manton et al., 1992 |
| Loewe Massif | 91286407 | charnockite | SHRIMP zircon | 980 ± 21 | | Kinny et al., 1997 |
| Mt McCarthy | 91286403 | leucogneiss | SHRIMP zircon | 990 ± 30 (anatexis) | | Kinny et al., 1997 |
| Mt Collins | 91286419 | granite | SHRIMP zircon | 976 ± 25 | | Kinny et al., 1997 |
| | 91286420 | granite | SHRIMP zircon | 984 ± 7 | | Kinny et al., 1997 |
| | 91286421 | quartz syenite | SHRIMP zircon | 984 ± 12 | | Kinny et al., 1997 |
| Mt Kirkby | CC2 | pegmatite | SHRIMP zircon | 991 ± 22 | | Carson et al., 2000 |
| | C16 | pegmatite | SHRIMP zircon | 910 ± 18 | | Carson et al., 2000 |
| | CC4 | pegmatite | SHRIMP zircon | 517 ± 12 | | Carson et al., 2000 |
| | CC5 | pegmatite | SHRIMP zircon | 1013 ± 31 (inherited) | | Carson et al., 2000 |
| Radok Lake | 9628-196 | leucosome | SHRIMP zircon | 1017 ± 31 | 900 ± 28 | Boger et al., 2000 |
| | 9628-73 | leucosome | SHRIMP zircon | 942 ± 17 | | Boger et al., 2000 |
| | 9628-141 | granite sheet | SHRIMP zircon | 990 ± 18 | | Boger et al., 2000 |
| | 9628-142 | granite dyke | SHRIMP zircon | 936 ± 14 | | Boger et al., 2000 |
| Loewe Massif | 9628-68 | pegmatite | SHRIMP zircon | 548 ± 4 | | Boger et al., 2002 |
| Radok Lake | 35153 | gneissic granite | ID-TIMS zircon | 1071 ± 23 | | Kamenev et al., 2009 |
| | 35301-3 | migmatite | ID-TIMS monazite | | 929 ± 3 | Kamenev et al., 2009 |
| Porthos Range | 35068 | felsic orthogneiss | ID-TIMS zircon | 1044 ± 10 | | Mikhalsky and Sheraton, 2011 |
| Stinear Nunataks | Stin-1A | paragneiss | LA-ICP-MS monazite | | 920 ± 7 | Morrissey et al., 2015 |
| Mt Dovers | 77199 | paragneiss | LA-ICP-MS monazite | | 944 ± 8 | Morrissey et al., 2015 |
| Hunt Nunataks | HN-3 | paragneiss | LA-ICP-MS monazite | | 1018 ± 8; 934 ± 8 | Morrissey et al., 2015 |
| Fox Ridge | Fox-5B | paragneiss | LA-ICP-MS monazite | | 902 ± 7 | Morrissey et al., 2015 |
| Mt Lanyou | 72523 | paragneiss | LA-ICP-MS monazite | | 1016 ± 8 | Morrissey et al., 2015 |
| Depot Peak | DP-1 | pegmatite | LA-ICP-MS monazite | | 487 ± 3 | Morrissey et al., 2016 |
| | DP-11 | pegmatite | LA-ICP-MS monazite | | 499 ± 3 | Morrissey et al., 2016 |
| | DP-7 | paragneiss | LA-ICP-MS monazite | | 928 ± 28; 532 ± 5 | Morrissey et al., 2016 |
| Else Platform | PCM-83 | paragneiss | LA-ICP-MS monazite | | 872 ± 31; 519 ± 5 | Morrissey et al., 2016 |
| Taylor Platform | 77090 | paragneiss | LA-ICP-MS monazite | | 517 ± 4 | Morrissey et al., 2016 |
| Brocklehurst Ridge | 77102B | paragneiss | LA-ICP-MS monazite | | 516 ± 4 | Morrissey et al., 2016 |
| Mt Meredith | 77079 | granofels | LA-ICP-MS monazite | | 504 ± 3 | Morrissey et al., 2016 |
| Loewe Massif | BL01-1 | charnockite | SHRIMP zircon | 949 ± 9 | | This paper |
| | BL04-1 | charnockite | SHRIMP zircon | 1050 ± 11 | 930 ± 9 | This paper |
| | BL07-3 | felsic orthogneiss | SHRIMP zircon | 1070 ± 14 | 921 ± 9 | This paper |
| Radok Lake | BL09-4 | felsic orthogneiss | SHRIMP zircon | 1150 ± 10 | 915 ± 12 | This paper |
| | BL10-1 | felsic orthogneiss | SHRIMP zircon | 1167 ± 18 | 946 ± 13 | This paper |
| | BL10-4 | felsic orthogneiss | SHRIMP zircon | 1096 ± 19 | 922 ± 16 | This paper |
| | BL10-2 | mafic granulite | SHRIMP zircon | | 914 ± 5 | This paper |
| | BL13-3 | mafic granulite | SHRIMP zircon | | 914 ± 5 | This paper |
| | BL14-1 | paragneiss | SHRIMP zircon | | 930 ± 15 | This paper |
| Else Platform | BL15-3 | paragneiss | SHRIMP zircon | | 910 ± 92; 520 ± 5 | This paper |
| *Mawson Coast* | | | | | | |
| Mawson Station | 80285049 | charnockite | ID-TIMS zircon | 935 + 3700/-12 | | Black et al., 1987 |
| Ufs Island | z644 | charnockite | SHRIMP zircon | 985 ± 29 | | Young and Black, 1991 |
| Falla Bluff | z542 | charnockite | SHRIMP zircon | 954 ± 12 | | Young and Black, 1991 |
| Mawson Station | z687 | gneissic xenolith | SHRIMP zircon | | 921 ± 19 | Young and Black, 1991 |
| Cape Bruce | C and R | orthogneiss | SHRIMP zircon | ca. 995 | | Dunkley et al., 2002 |
| | B | orthogneiss dyke | SHRIMP zircon | 992 ± 10 | | Dunkley et al., 2002 |
| | F | felsic dyke | SHRIMP zircon | 937 ± 19 | | Dunkley et al., 2002 |
| | D | pegmatite | SHRIMP zircon | 909 ± 7 | | Dunkley et al., 2002 |

(*continued on next page*)

**Table 3** (*continued*)

| Location | Sample | Rock type | Dating method | Magmatic age (Ma) | Metamorphic age (Ma) | Reference |
|---|---|---|---|---|---|---|
| Mawson Station | 90030 | charnockite | LA-ICP-MS zircon | 982 ± 33 Ma | | Halpin et al., 2005 |
| Cape Bruce | AC34 | paragneiss | CHIME monazite | | 930 ± 12; 924 ± 10; 915 ± 13 | Halpin et al., 2007 |
| Forbes Glacier | 90024 | paragneiss | CHIME monazite | | 969 ± 14; 939 ± 12; 909 ± 6 | Halpin et al., 2007 |
| Macey Island | LM01 | charnockite | LA-ICP-MS zircon | 1145 ± 11 Ma | | Halpin et al., 2012 |
| Austskjeka | ML11 | charnockite | LA-ICP-MS zircon | 1140 ± 22 Ma | | Halpin et al., 2012 |
| Chapman Ridge | RW28 | charnockite | LA-ICP-MS zircon | 1078 ± 17 Ma | | Halpin et al., 2012 |
| Macklin Island | LM12 | charnockite | LA-ICP-MS zircon | 1048 ± 39 Ma | | Halpin et al., 2012 |
| Mawson Station | LM53 | charnockite | LA-ICP-MS zircon | 984 ± 14 Ma | | Halpin et al., 2012 |
| Mt Horden | LF60 | charnockite | LA-ICP-MS zircon | 961 ± 16 Ma | | Halpin et al., 2012 |
| David Range | JF37 | felsic gneiss | LA-ICP-MS zircon | | 986 ± 32 | Halpin et al., 2013 |
| Cape Bruce | AC34 | paragneiss | LA-ICP-MS zircon | | 941 ± 9 Ma | Halpin et al., 2013 |
| Forbes Glacier | 90024 | paragneiss | LA-ICP-MS zircon | | 961 ± 17 Ma | Halpin et al., 2013 |

Protoliths of felsic orthogneisses were formed at ca. 1170–1070 Ma.

oscillatory bands in some zircon cores. The other three age populations were obtained from well-preserved oscillatory-zoned zircon cores and therefore reflect three magmatic episodes in the source region. The ca. 2130–1850 Ma detrital zircons have been identified in paragneisses from Mount Meredith, the Foster Nunatak, the Mawson Coast and the Grove Mountains (Young and Black, 1991; Kinny et al., 1997; Liu et al., 2007b; Halpin et al., 2013; Mikhalsky et al., 2016; Wang et al., 2016). This points to the existence of the Paleoproterozoic crust in the source region, and the low $\varepsilon_{Hf}(t)$ values (−10.8 to +2.0) and old $T_{DM2}^{Hf}$ ages (2.50–3.18 Ga) indicate a derivation of Archean source components for this crust. The ca. 1800–1600 Ma detrital zircons were also found in metasedimentary rocks in the Larsemann Hills, the Grove Mountains and the EGB of India (Wang et al., 2008; Bose et al., 2011; Grew et al., 2012; Wang et al., 2016). Furthermore, it has been shown that some charnockitic and anorthositic intrusives from the EGB were emplaced during the period ca. 1760–1630 Ma (Kovach et al., 2001; Bose et al., 2011; Dharma Rao et al., 2012). Thus, the EGB may have provided the source materials for paragneisses from the Rayner Complex. The ca. 1480–1140 Ma detrital zircons comprise almost two-third of the dataset and correspond with the main period of magmatism in the Rayner Complex (Black et al., 1987; Liu et al., 2007a, 2009, 2014, 2016; Wang et al., 2008; Grew et al., 2012; Halpin et al., 2012; Mikhalsky et al., 2013). This seems to suggest that most detritus of the paragneisses were derived directly from the active Indian continental margin/the Rayner continental magmatic arc. However, the bimodal $T_{DM2}^{Hf}$ ages (2.3–1.9 and 3.0–2.4 Ga) of these detrital zircons indicate an addition of remelted products of an older Archean/early Paleoproterozoic source region. The mean age of ca. 1200 Ma obtained for the 12 youngest detrital zircon grains defines the sedimentation occurring before arc magmatism (ca. 1170–1020 Ma) in the northern PCM.

Detrital zircons from sample BL15-3 collected from the Else Platform show a major age population at ca. 1180–830 Ma and a subordinate age population at ca. 1370–1230 Ma. The subordinate age population coincides with the major age population of sample BL14-1 (ca. 1480–1140 Ma), and the $T_{DM2}^{Hf}$ ages (2.8–2.1 Ga for sample BL15-3) of the two samples are also comparable. This suggests that some detrital materials from these two samples share the same provenance. The major age population of sample BL15-3 overlaps with the age range of magmatism and metamorphism in the northern PCM, suggesting partial or even complete Pb loss for some zircon grains during metamorphism. In support of this inference, the oscillatory bands in many zircon cores from this sample have been thickened, blurred, or even entirely homogenized, reflecting varying degrees of solid-state recrystallization. Thus, care should be taken in determining the depositional ages of metasedimentary rocks in the high-grade metamorphic terranes. In the present case, considering the age population peaks at ca. 1020 Ma, we infer that deposition of the paragneiss precursor took place after the arc magmatism (ca. 1170–1020 Ma) and immediately before metamorphism (ca. 945–915 Ma; see below), much like the metaquartzite from the Larsemann Hills (Grew et al., 2012). However, a clear difference in zircon Hf isotopic compositions between the paragneiss and the associated felsic orthogneisses (and potentially contemporaneous mafic granulites) (negative $\varepsilon_{Hf}(t)$ values and older $T_{DM2}^{Hf}$ ages versus positive $\varepsilon_{Hf}(t)$ values and younger $T_{DM2}^{Hf}$ ages; see Fig. 10) demonstrates that the latter was not the direct source of the former.

In summary, the paragneisses from the Rayner Complex may have received detritus mainly from the active Indian continental margin/the Rayner continental arc, and deposition was approximately contemporaneous with the late Mesoproterozoic arc magmatism. The depositional environment may have been intra-arc basins (Liu et al., 2014, 2016), or a back-arc basin as inferred for

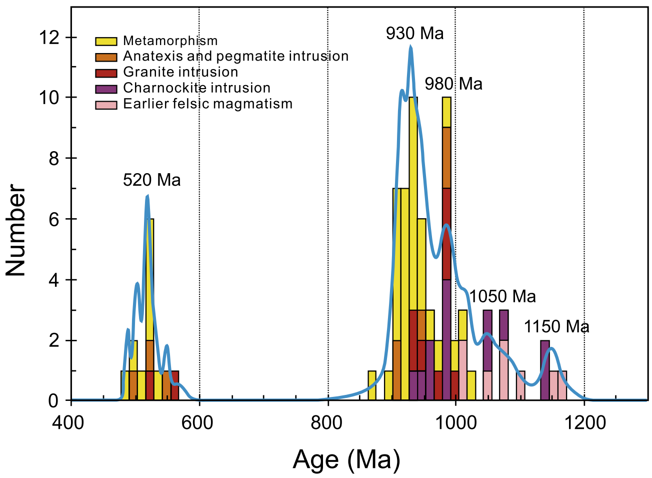


**Fig. 12.** Cumulative probability histogram of published zircon and monazite U–Pb age data from the northern Prince Charles Mountains and adjacent Mawson Coast.

equivalent paragneisses from the Mawson Coast (Halpin et al., 2013) and for boron- and phosphate-rich paragneisses from the Larsemann Hills (Grew et al., 2013).

### 8.3. Emplacement ages of charnockites

Charnockites are widely distributed along the Mawson Coast (called the Mawson Charnockite) and were previously dated at 985 ± 29 to 935 + 3700/−12 Ma using zircon U–Pb geochronology (Black et al., 1987; Young and Black, 1991; Halpin et al., 2005) (see Table 3). A similar age of 980 ± 21 Ma was also obtained for charnockites from the Loewe Massif of the northern PCM (Kinny et al., 1997). Considering the nature of their deformation, the intrusion of these charnockites was commonly thought to be nearly contemporaneous with regional high-grade metamorphism (Young and Black, 1991; Kinny et al., 1997; Boger et al., 2000; Carson et al., 2000). The subsequent dating of charnockites from the Reinbolt Hills and the Gillock Island of the eastern Amery Ice Shelf (955 ± 13 and 979 ± 11 Ma, respectively; Liu et al., 2009; Mikhalsky and Kamenev, 2013) supports this interpretation. However, recent LA–ICP–MS U–Pb zircon dating on the Mawson Charnockite revealed three emplacement episodes at ca. 1145–1140, ca. 1080–1050 and ca. 985–960 Ma (Halpin et al., 2012), indicating a complexity in the timing and nature of charnockitic magmatism in the Rayner orogen.

Our new SHRIMP U–Pb zircon dating for two charnockite samples from the Loewe Massif also gave dissimilar results. The different textural domains in zircons from massive sample BL01-1 yield an indistinguishable age of 949 ± 9 Ma. This age broadly brackets the younger age group mentioned above and is commonly interpreted to represent the minimum emplacement age of the charnockite. However, based on the criteria proposed by Halpin et al. (2012), the minimum emplacement age for this sample might be as old as ca. 970 Ma, whereas the weighted mean age is likely to reflect the effect of late metamorphism. In contrast, the different textural domains in zircons from foliated sample BL04-1 yield two distinct weighted mean ages: 1050 ± 11 Ma for the oscillatory-zoned cores and 930 ± 9 Ma for the overgrowth rims. In general, the former is regarded as a protolith emplacement age and the latter as a metamorphic age. The growth of garnet clearly indicates a metamorphic overprint on this sample and appears to support this interpretation. Moreover, sample BL04-1 contains several older zircon inner cores of ca. 1490–1240 Ma, which are probably xenocrysts from the country rocks.

Given that both samples BL01-1 and BL04-1 were collected from the northern Loewe Massif and that they are only 6 km apart, it is anomalous that their emplacement ages differ by nearly 100 Myr. The most likely explanation for this is that the two samples represent two different charnockite bodies. The minor difference in Hf isotopic compositions between the charnockites and surrounding felsic orthogneisses suggests that they were generated within a similar Paleoproterozoic source region, but that the partial melting to generate charnockitic magma probably occurred at deeper levels (Young et al., 1997). If this is the case, it would be worth investigating whether the two earlier episodes of charnockitic magmatism, which are virtually contemporaneous with two phases of felsic magmatism (1150 and 1050 Ma; Fig. 12), were also intruded in a continental arc setting. Another possibility for the age difference between the two samples is that sample BL04-1 was taken from the margin of the charnockite body, where it may have suffered strong assimilation/contamination with country rocks during magma generation or intrusion. In such a case, all older oscillatory-zoned zircon grains would likely to be xenocrysts and therefore have Hf isotopic signatures similar to those of the country rocks. The oldest age of 981 ± 24 Ma from 3 younger oscillatory-zoned zircon grains may represent the actual emplacement age of the charnockite (Halpin et al., 2012).

### 8.4. Reappraisal of the timing of late Mesoproterozoic/early Neoproterozoic metamorphism

The U–Pb dating of zircon overgrowth domains from felsic orthogneisses and paragneisses as well as individual zircons from mafic granulites from the Beaver Lake area yield weighted mean $^{207}Pb/^{206}Pb$ or $^{206}Pb/^{238}U$ ages between 946 ± 13 and 914 ± 5 Ma. The dated zircon domains commonly show weak or strong luminescence with relatively homogeneous internal structure or sector/fir-tree zoning. Thus, we interpret the resulting ages (ca. 945–915 Ma) to represent the timing of zircon growth during metamorphism in the northern PCM. With the exception of a few zircon rims from felsic orthogneiss sample BL07-3 and paragneiss sample BL14-1, most zircon overgrowth domains have high Th/U ratios (generally > 0.20) that are similar to the Th/U ratios of metamorphic zircons from other granulite terranes (Vavra et al., 1999; Möller et al., 2003). Previously available U–Pb zircon data for the Rayner Complex suggest a wide spread of ages between ca. 930 and 900 Ma (Grew and Manton, 1981; Young and Black, 1991; Boger et al., 2000; Carson et al., 2000; Liu et al., 2009, 2014, 2016; Mikhalsky et al., 2013), whereas in situ U–Th–Pb monazite ages of metapelites from the northern PCM and the Mawson Coast are also concentrated at ca. 940–900 Ma (Halpin et al., 2007a; Morrissey et al., 2015). Our new SHRIMP U–Pb zircon geochronology for the various metamorphic rock types from the Beaver Lake area produces similar results, suggesting that both zircons and monazites of metamorphic origin in the Rayner Complex grew more concentratedly in the period ca. 940–900 Ma.

However, previous geochronological studies on the Rayner Complex conclude that a protracted late Mesoproterozoic/early Neoproterozoic high-grade metamorphic event continued from ca. 1000 to ca. 900 Ma (Black et al., 1987; Sheraton et al., 1987; Grew et al., 1988; Young and Block, 1991; Boger et al., 2000; Dunkley et al., 2002; Halpin et al., 2007a). In these studies, the peak metamorphic ages of ca. 1000–980 Ma were mainly speculated from earlier deformation [D1 and D2 of Boger et al. (2000)] and the U–Pb zircon dating of structurally constrained charnockites, granites, leucosomes and pegmatites (Young and Black, 1991; Kinny et al., 1997; Carson et al., 2000; Boger et al., 2000; Dunkley, 1998; Dunkley et al., 2002) (see Table 3), whereas metamorphic zircon overgrowths of >945 Ma were only identified in a felsic gneiss and a paragneiss from the Mawson Coast (Halpin et al., 2013) and in some felsic orthogneisses from the eastern Amery Ice Shelf–southwestern Prydz Bay area (Liu et al., 2009, 2014). Although an upper intercept age of 1000 + 14/−11 Ma obtained for a felsic gneiss from the Else Platform was interpreted as a metamorphic age (Manton et al., 1992), this interpretation was not constrained by zircon internal structure or chemistry. However, an earlier monazite growth episode at ca. 1020 Ma was recently recognized from paragneisses from both the northern PCM and EGB (Bose et al., 2011; Morrissey et al., 2015), suggesting the onset of metamorphism as early as ca. 1020 Ma. In any case, two remarkable age populations at ca. 1020–970 Ma (peak at 980 Ma) and ca. 945–900 Ma (peak at 930 Ma) (see Fig. 12) and the distinction of deformation features in each of those periods (Carson et al., 2000; Boger et al., 2000) imply that late Mesoproterozoic/early Neoproterozoic high-grade metamorphism might have taken place episodically.

As previously reported, two-stage reaction textures in metamorphic rocks from the northern PCM and the Mawson Coast document late Mesoproterozoic/early Neoproterozoic medium- to low-pressure granulite facies metamorphism followed by a near-isobaric cooling path (Clarke et al., 1989; Fitzsimons and Harley, 1992, 1994; Thost and Henson, 1992; Hand et al., 1994a; Nichols, 1995; Scrimgeour and Hand, 1997; Stephenson and Cook, 1997; Dunkley, 1998; Boger and White, 2003; Halpin et al., 2007a; Morrissey et al., 2015). However, it is unclear whether the two-stage metamorphism and the two age populations correspond one-to-one. Garnet-hosted monazites from metapelites along the Mawson Coast yield an age of ca. 970 Ma, whereas monazites hosted by other mineral grains and in the matrix produce ages of ca. 940–910 Ma (Halpin et al., 2007a). In combination with the dating of nearby structurally constrained felsic intrusives, peak metamorphism was thought to have occurred at ca. 990–970 Ma, and subsequent near-isobaric cooling were slow, sustaining for ca. 80 Myr (Halpin et al., 2007a). Similar results led to similar interpretations for metapelites from the northern PCM, although the garnet-hosted monazites in this area yield somewhat older ages of ca. 1020 Ma (Morrissey et al., 2015). A comparable two-stage metamorphic evolution was developed in mafic granulites and paragneisses from Mount Brown. However, zircon U–Pb dating suggest the commencement of metamorphism no earlier than ca. 920–900 Ma (Liu et al., 2016). Monazites from different textural sites, including those enclosed in garnet, in paragneisses from this area also yield similar age results (Liu et al., in prep.). This implies that the ca. 920–900 Ma metamorphism represent a single granulite facies metamorphic episode that was accompanied by a near-isobaric cooling *P*–*T* path. In fact, the two-stage growth of garnet observed in charnockite sample BL04-1 probably also occurred in this time.

### 8.5. On late Neoproterozoic/Cambrian reworking

Unlike the area east of the Lambert Graben, late Neoproterozoic/Cambrian reworking in the northern PCM was thought to be of only minor importance and was assumed to be restricted to discrete NE-trending mylonitic zones that commonly occur on the margins of the ca. 550–500 Ma pegmatites (Manton et al., 1992; Carson et al., 2000; Boger et al., 2002). The metamorphic reworking is lower grade, with *P*–*T* conditions of 524 ± 20 °C and 7.6 ± 4 kbar (Fitzsimons and Thost, 1992; Boger et al., 2002). The renewed growth of zircon during this period has not been described in metamorphic rocks (Manton et al., 1992; Kinny et al., 1997). However, recent phase equilibrium modelling and in situ LA–ICP–MS U–Pb dating of microstructurally controlled monazites from some metapelites in the northern PCM clearly show a patchy high-temperature (800–870 °C at 5.5–6.5 kbar) metamorphic overprinting of the basement during the Cambrian (532 ± 5 to 504 ± 3 Ma; Morrissey et al., 2016). Our new SHRIMP U–Pb zircon dating indicates no or only very little Pb loss for zircon grains from most samples. An exception is paragneiss sample BL15-3 from Else Platform, in which a single sector-zoned zircon grain of 531 ± 13 Ma and an overgrowth rim of 520 ± 5 Ma were recognized. Since the CL features and Th/U ratios of these zircon domains are similar to those of the ca. 945–915 Ma zircon overgrowths described above, it is difficult to determine whether the young ages resulted from the complete isotopic resetting of early Neoproterozoic zircons or new zircon growth. Nevertheless, late Neoproterozoic/Cambrian metamorphic reworking in the northern PCM has been verified by U–Pb zircon geochronology.

### 8.6. Implications for the Rayner orogeny

The timing and sequence of magmatic, sedimentary and metamorphic events in the northern PCM are comparable to those in other parts of the Rayner Complex. Regionally, the earliest magmatic episode at ca. 1490–1400 Ma occurred in Enderby Land adjacent to the Archean Napier Complex (Black et al., 1987), and Mount Brown east of Archean/early Paleoproterozoic Vestfold Block (Mikhalsky et al., 2015; Liu et al., 2016). A subsequent magmatic episode at ca. 1380–1320 Ma was identified in the Munro Kerr Mountains and the Luff Nunatak of the eastern Amery Ice Shelf (Liu et al., 2009, 2014) and the Mount Lanyon in the northern PCM (Mikhalsky et al., 2013; unpublished data). Considering that the Kanigiri ophiolite mélange discovered in between the Dharwar craton and the EGB has been dated at ca. 1330–1300 Ma (Dharma Rao et al., 2011), we infer that these two arc-related magmatic episodes occurred on the active Indian continental margin during the early Mesoproterozoic. The magmatic episode at ca. 1210–1020 Ma dominates the northern PCM-Prydz Bay region and was accompanied by charnockite intrusion in the northern PCM and on the Mawson Coast. The tectonic setting for this magmatism has converted from an Andean-type active continental margin to a continental arc system (i.e., the Rayner continental arc) separated by an oceanic or back-arc basin from the Indian craton. Detritus derived mainly from the active continental margin/continental arc was deposited in intra-arc or back-arc basins before, during or after magmatism. At the same time, an isotopically juvenile Fisher arc and a slightly younger Clemence arc may have formed to the south of the Rayner continental arc (Mikhalsky et al., 1996, 2006a,b; Liu et al., 2013, 2014). Together, the events outlined above document the activity of a long-lived (ca. 1490 to ca. 1020 Ma) subduction–accretion system between the Indian craton and East Antarctica.

As mentioned before, zircon and monazite growth episodically at ca. 1020–970 and ca. 940–900 Ma seems to be consistent throughout much of the Rayner Complex. Except for a protracted metamorphic model as advocated by some workers (e.g., Boger et al., 2000; Halpin et al., 2007a; Morrissey et al., 2015), an alternative episodic metamorphic model that is related to two-stage collision between the Indian craton and East Antarctica can or should be taken into account in the interpretation of the present age data (e.g., Kelly et al., 2002; Liu et al., 2013, 2014). The ca. 1020–970 Ma metamorphic episode was accompanied by the development of contemporaneous compressional deformation and the intrusion of charnockitic and granitic magmas, and is therefore likely to be the result of the collision of the three island arcs (i.e., the Rayner, Fisher and Clemence arcs) with East Antarctica (Liu et al., 2013, 2014). The ca. 940–900 Ma metamorphic episode dominates the Rayner Complex and is the only metamorphic episode observed in the reworked Napier Complex in Kemp Land (Kelly et al., 2002; Halpin et al., 2007b). This signifies the closure of the ocean or back-arc basin and the final amalgamation of the Indian craton and the newly accreted East Antarctic continental margin. Overall, the tectonics of the Rayner orogeny evolved from arc accretion, through arc-continent collision to continent–continent collision during the period ca. 1500–900 Ma. The absence of high- or ultrahigh-pressure metamorphic rocks reflects soft collision during convergent orogeny. Therefore, like the Neoproterozoic–Paleozoic Central Asian Orogenic Belt between the Siberian and North China cratons (Sengör et al., 1993; Jahn, 2004; Kröner et al., 2014), the Rayner orogen seems to represent another long-lived accretionary orogen that the orogenic root was exposed on the Earth's surface.

## 9. Conclusions

(1) The protoliths of the felsic orthogneisses from the Beaver Lake area of the northern PCM formed at ca. 1170–1070 Ma, followed by two separate episodes of charnockite emplacement at ca. 1050 and ca. 950 Ma or a single episode at ca. 980 Ma. Similarities in the Hf isotopic compositions of these two rock types suggest that they were derived from the same Paleoproterozoic source, but that the partial melting to generate charnockite magma occurred at deeper levels.

(2) Detrital zircons from two paragneiss samples yield slightly different age spectra, indicating their deposition before and after the intrusion of felsic orthogneisses protoliths, respectively. The metasedimentary precursors received detritus mainly from the active Indian continental margin/the Rayner continental arc, but have not been derived from the surrounding felsic orthogneisses and mafic granulites.

(3) The late Mesoproterozoic/early Neoproterozoic high-grade metamorphism of the Rayner Complex was probably episodic at ca. 1020–970 and 940–900 Ma. The late metamorphic episode led to the extensive growth of zircon and monazite, and probably represents the main period of regional metamorphism. The zircon record for Cambrian metamorphic reworking was only observed in a single paragneiss samples from the Else Platform.

(4) The timing and sequence of magmatic, sedimentary and metamorphic events in the northern PCM are comparable with those in other parts of the Rayner Complex. The available data demonstrate the tectonic evolution of the Rayner orogen between ca. 1500 and 900 Ma from accretion to collision. Therefore, the Rayner orogen essentially represents a long-lived accretionary orogen that the orogenic root was exposed on the Earth's surface.

## Acknowledgements

We thank Jian Liu, Yingchun Cui and James Hamilton for assistance during 12 day's fieldwork in the northern Prince Charles Mountains during the 2014–2015 Chinese National Antarctic Research Expedition. Logistic support from the Australian Antarctic Division and the Chinese Arctic and Antarctic Administration are gratefully acknowledged. Critical reviews by E. V. Mikhalsky and Yanbin Wang substantially improved the manuscript. This research was supported by the National Natural Science Foundation of China (No. 41530209), the Chinese Polar Environment Comprehensive investigation & Assessment Programmes (No. CHINARE2016-02-05) and the Geological Investigation Project of the Chinese Geological Survey (No. 12120113019000).

## Appendix A. Supplementary data

Supplementary data associated with this article can be found, in the online version, at http://dx.doi.org/10.1016/j.precamres.2017.07.012.

## References


Andersen, T., 2002. Correction of common lead in U–Pb analyses that do not report 204 Pb. Chem. Geol. 192, 59–79.

Beliatsky, B.V., Laiba, A.A., Mikhalsky, E.V., 1994. U-Pb zircon age of the metavolcanic rocks of Fisher Massif (Prince Charles Mountains, East Antarctica). Antarct. Sci. 6, 355–358.

Black, L.P., Harley, S.L., Sun, S.S., Mcculloch, M.T., 1987. The Rayner Complex of East Antarctica: complex isotopic systematics within a Proterozoic mobile belt. J. Metamorph. Geol. 5, 1–26.

Black, L.P., Kamo, S.L., Allen, C.M., Aleinikoff, J.N., Davis, D.W., Korsch, R.J., Foudoulis, C., 2003. TEMORA 1: a new standard for Phanerozoic U-Pb geochronology. Chem. Geol. 200, 155–170.

Blichert-Toft, J., Chauvel, C., Albarède, F., 1997. Separation of Hf and Lu for high-precision isotope analysis of rock samples by magnetic sector-multiple collector ICP–MS. Contrib. Miner. Petrol. 127, 248–260.

Boger, S.D., 2011. Antarctica—before and after Gondwana. Gondwana Res. 19, 335–371.

Boger, S.D., White, R.W., 2003. The metamorphic evolution of metapelitic granulites from Radok Lake, northern Prince Charles Mountains, east Antarctica: evidence for an anticlockwise P-T path. J. Metamorph. Geol. 21, 285–298.

Boger, S.D., Wilson, C.J.L., 2005. Early Cambrian crustal shortening and a clockwise P-T–t path from the southern Prince Charles Mountains, East Antarctica: implications for the formation of Gondwana. J. Metamorph. Geol. 23, 603–623.

Boger, S.D., Carson, C.J., Wilson, C.J.L., Fanning, C.M., 2000. Neoproterozoic deformation in the northern Prince Charles Mountains, East Antarctica: evidence for a single protracted orogenic event. Precambr. Res. 104, 1–24.

Boger, S.D., Carson, C.J., Fanning, C.M., Hergt, J.M., Wilson, C.J.L., Woodhead, J.D., 2002. Pan-African intraplate deformation in the northern Prince Charles Mountains, East Antarctica. Earth Planet. Sci. Lett. 195, 195–210.

Bose, S., Dunkley, D.J., Dasgupta, S., Das, K., Arima, M., 2011. India–Antarctica–Australia–Laurentia connection in the Paleoproterozoic-Mesoproterozoic revisited: evidence from the Eastern Ghats Belt, India. Geol. Soc. Am. Bull. 123, 2031–2049.

Bouvier, A., Vervoort, J.D., Patchett, P.J., 2008. The Lu–Hf and Sm–Nd isotopic composition of CHUR: constraints from unequilibrated chondrites and implications for the bulk composition of terrestrial planets. Earth Planet. Sci. Lett. 273, 48–57.

Carson, C.J., Fanning, C.M., Wilson, C.J.L., 1996. Timing of the Progress Granite, Larsemann Hills: evidence for Early Palaeozoic orogenesis within the East Antarctica Shield and implications for Gondwana assembly. Aust. J. Earth Sci. 43, 539–553.

Carson, C.J., Boger, S.D., Fanning, C.M., Wilson, C.J.L., Thost, D.E., 2000. SHRIMP U-Pb geochronology from Mount Kirkby, northern Prince Charles Mountains, East Antarctica. Antarct. Sci. 12, 429–442.

Clarke, G.L., Powell, R., Guiraud, M., 1989. Low-pressure granulite facies metapelitic assemblages and corona textures from Mac. Robertson Land, East Antarctica: the importance of $Fe_2O_3$ and $TiO_2$ in accounting for spinel-bearing assemblages. J. Metamorph. Geol. 7, 323–335.

Dharma Rao, C.V., Santosh, M., Wu, Y.B., 2011. Mesoproterozoic ophiolitic mélange from the SE periphery of the Indian plate: U-Pb zircon ages and tectonic implications. Gondwana Res. 19, 384–401.

Dharma Rao, C.V., Santosh, M., Dong, Y., 2012. U-Pb zircon chronology of the Pangidi-Kondapalle layered intrusion, Eastern Ghats Belt, India: constraints on Mesoproterozoic arc magmatism in a convergent margin setting. J. Asian Earth Sci. 49, 362–375.

Dunkley, D.J., The Rayner Complex in MacRobertson Land, east Antarctica. Ph.D. thesis, The University of Sydney, Sydney, 1998, pp. 1–284.

Dunkley, D.J., Clarke, G.L., White, R.W., 2002. Structural and metamorphic evolution of the mid-late Proterozoic Rayner Complex, Cape Bruce, East Antarctica. In: Gamble, J.A., Skinner, D.N.B., Henrys, S. (Eds.), Antarctica at the Close of a Millennium, 35. The Royal Society of New Zealand, pp. 31–42.

Fisher, C.M., Vervoort, J.D., Hanchar, J.M., 2014. Guidelines for reporting zircon Hf isotopic data by LA–MC–ICPMS and potential pitfalls in the interpretation of these data. Chem. Geol. 363, 125–133.

Fitzsimons, I.C.W., 2000. Grenville-age basement provinces in East Antarctica: evidence for three separate collisional orogens. Geology 28, 879–882.

Fitzsimons, I.C.W., 2003. Proterozoic basement provinces of southern and southwestern Australia, and their correlation with Antarctica. In: Yoshida, M., Windley, B., Dasgupta, S. (Eds.), Proterozoic East Gondwana: Supercontinent Assembly and Breakup. Geological Society, London, pp. 93–130. Special Publications 206.

Fitzsimons, I.C.W., Harley, S.L., 1992. Mineral reaction textures in high grade gneisses, evidence for contrasting pressure–temperature paths in the Proterozoic complex of east Antarctica. In: Yoshida, Y., Kaminuma, K., Shiraishi, K. (Eds.), Recent Progress in Antarctic Earth Science. Terra Scientific Publishing Company, Tokyo, pp. 103–111.

Fitzsimons, I.C.W., Thost, D.E., 1992. Geological relationships in high-grade basement gneiss of the northern Prince Charles Mountains, East Antarctica. Aust. J. Earth Sci. 39, 173–193.

Fitzsimons, I.C.W., Harley, S.L., 1994. Garnet coronas in scapolite–wollastonite calc-silicates from East Antarctica: the application and limitation of activity corrected grids. J. Metamorph. Geol. 12, 761–777.

Fitzsimons, I.C.W., Kinny, P.D., Harley, S.L., 1997. Two stages of zircon and monazite growth in anatectic leucogneiss: SHRIMP constraints on the duration and

intensity of Pan-African metamorphism in Prydz Bay, East Antarctica. Terra Nova 9, 47–51.
Grew, E.S., Manton, W.I., 1981. Geochronologic studies in East Antarctica: ages of rocks at Reinbolt Hills and Molodezhnaya Station. Antarct. J. United States 16, 5–7.
Grew, E.S., Manton, W.I., James, P.R., 1988. U-Pb data on granulite facies rocks from Fold Island, Kemp Coast, East Antarctica. Precambr. Res. 42, 63–75.
Grew, E.S., Carson, C.J., Christy, A.G., Maas, R., Yaxley, G.M., Boger, S.D., Fanning, C. M., 2012. New constraints from U-Pb, Lu–Hf and Sm–Nd isotopic data on the timing of sedimentation and felsic magmatism in the Larsemann Hills, Prydz Bay, East Antarctica. Precambr. Res. 206–207, 87–108.
Grew, E.S., Carson, C.J., Christy, A.G., Boger, S.D., 2013. Boron- and phosphate-rich rocks in the Larsemann Hills, Prydz Bay, East Antarctica: tectonic implications. In: Harley, S.L., Fitzsimons, I.C.W., Zhao, Y. (Eds.), Antarctica and Supercontinent Evolution. Geological Society, London, pp. 73–94. Special Publication 283.
Griffin, W.L., Wang, X., Jackson, S.E., Pearson, N.J., O'Reilly, S.Y., Xu, X.S., Zhou, X.M., 2002. Zircon chemistry and magma mixing, SE China: in-situ analysis of Hf isotopes, Tonglu and Pingtan igneous complexes. Lithos 61, 237–269.
Halpin, J.A., Gerakiteys, C.L., Clarke, G.L., Belousova, E.A., Griffin, W.L., 2005. In-situ U-Pb geochronology and Hf isotope analyses of the Rayner Complex, east Antarctica. Contrib. Miner. Petrol. 148, 689–706.
Halpin, J.A., Clarke, G.L., White, R.W., Kelsey, D.E., 2007. Contrasting P-T–t Paths for Neoproterozoic metamorphism in MacRobertson and Kemp Lands, East Antarctica. J. Metamorph. Geol. 25, 683–701.
Halpin, J.A., White, R.W., Clarke, G.L., Kelsey, D.E., 2007. The Proterozoic P-T–t evolution of the Kemp Land coast, East Antarctica: constraints from Si-saturated and Si-undersaturated metapelites. J. Petrol. 48, 1321–1349.
Halpin, J.A., Daczko, N.R., Milan, L.A., Clarke, G.L., 2012. Decoding near-concordant U-Pb zircon ages spanning several hundred million years: recrystallization, metamictisation or diffusion. Contrib. Miner. Petrol. 163, 67–85.
Halpin, J.A., Daczko, N.R., Clarke, G.L., Murray, K.R., 2013. Basin analysis in polymetamorphic terranes: an example from east Antarctica. Precambr. Res. 231, 78–97.
Hand, M., Scrimgeour, I., Powell, R., Stüwe, K., Wilson, C.J.L., 1994. Metapelitic granulites from Jetty Peninsula, east Antarctica: formation during a single event or by polymetamorphism? J. Metamorph. Geol. 12, 557–573.
Hand, M., Scrimgeour, I., Stüwe, K., Arne, D., Wilson, C.J.L., 1994. Geological observations in high grade mid-Proterozoic rocks from Else Platform, northern Prince Charles Mountains region, East Antarctica. Aust. J. Earth Sci. 41, 311–329.
Harley, S.L., 2003. Archaean-Cambrian crustal development of East Antarctica: metamorphic characteristics and tectonic implications. In: Yoshida, M., Windley, B., Dasgupta, S. (Eds.), Proterozoic East Gondwana: Supercontinent Assembly and Breakup. Geological Society, London, pp. 203–230. Special Publications 206.
He, X.X., Tang, S.H., Zhu, X.K., Wang, J.H., 2007. Precise measurement of Nd isotopic ratios by means of Multi-collector magnetic sector inductively coupled plasma mass spectrometry. Acta Geosci. Sin. 28, 405–410 (in Chinese with English abstract).
Hensen, B.J., Zhou, B., 1995. A Pan-African granulite facies metamorphic episode in Prydz Bay, Antarctica: evidence from Sm–Nd garnet dating. Aust. J. Earth Sci. 42, 249–258.
Hokada, T., Harley, S.L., Dunkley, D.J., Kelly, N.M., Yokoyama, K., 2016. Peak and post-peak development of UHT metamorphism at Mather Peninsula, Rauer Island: zircon and monazite U-Th–Pb and REE chemistry constraints. J. Mineral. Petrol. Sci. 111, 89–103.
Hu, Z.C., Liu, Y.S., Gao, S., Hu, S.H., Dietiker, R., Günther, D., 2008. A local aerosol extraction strategy for the determination of the aerosol composition in laser ablation inductively coupled plasma mass spectrometry. J. Anal. At. Spectrom. 23, 1192–1203.
Hu, Z.C., Liu, Y.S., Gao, S., Liu, W.G., Zhang, W., Tong, X.R., Lin, L., Zong, K.Q., Li, M., Chen, H.H., Zhou, L., Yang, L., 2012. Improved *in situ* Hf isotope ratio analysis of zircon using newly designed X skimmer cone and jet sample cone in combination with the addition of nitrogen by laser ablation multiple collector ICP–MS. J. Anal. At. Spectrom. 27, 1391–1399.
Jahn, B.-M., 2004. The Central Asian Orogenic Belt and growth of the continental crust in the Phanerozoic. In: Malpas, J., Fletcher, C.J.N., Ali, J.R., Aitchison, J.C. (Eds.), Aspects of the Tectonic Evolution of China. Geological Society, London, pp. 73–100. Special Publication 226.
Kamenev, E.N., Glebovitskii, V.A., Kovach, V.P., Semenov, V.S., Alekseev, N.L., Sal'nikova, E.B., Mikhailov, V.M., 2009. Late Precambrian metamorphic events in Eastern Antarctica. (Northern Prince Charles Mountains, Radok Lake Area, 70°52′ S, 67°57′ E). Dokl. Earth Sci. 425A, 380–383.
Kelly, N.M., Clarke, G.L., Fanning, C.M., 2002. A two-stage evolution of the Neoproterozoic Rayner Structural Episode: new U-Pb sensitive high resolution ion microprobe constraints from the Oygarden Group, Kemp Land, East Antarctica. Precambr. Res. 111, 307–330.
Kelsey, D.E., Powell, R., Wilson, C.J.L., Steele, D.A., 2003. (Th + U)–Pb monazite ages from Al–Mg-rich metapelites, Rauer Group, East Antarctica. Contrib. Miner. Petrol. 146, 326–340.
Keto, L.S., Jacobsen, S.B., 1987. Nd and Sr isotopic variations of Early Paleozoic oceans. Earth Planet. Sci. Lett. 84, 27–41.
Kinny, P.D., Black, L.P., Sheraton, J.W., 1997. Zircon U-Pb ages and geochemistry of igneous and metamorphic rocks in the northern Prince Charles Mountains, Antarctica. J. Aust. Geol. Geophys. 16, 637–654.
Kovach, V.P., Simmat, R., Rickers, K., Berezhnaya, N.G., Salnikova, E.B., Dobmeier, C., Raith, M.M., Yakovleva, S.Z., Kotov, A.B., 2001. The Western Charnockite Zone of the Eastern Ghats Belt, India: an independent crustal province of late Archean (2.8 Ga) and Paleoproterozoic (1.7–1.6 Ga) terrains. Gondwana Res. 4, 666–667.
Kröner, A., Kovach, V., Belousova, E., Hegner, E., Armstrong, R., Dolgopolova, A., Seltmann, R., Alexeiev, D.V., Hoffmann, J.E., Wong, J., Sun, M., Cai, K., Wang, T., Tong, Y., Wilde, S.A., Degtyarev, K.E., Rytsk, E., 2014. Reassessment of continental growth during the accretionary history of the Central Asian Orogenic Belt. Gondwana Res. 25, 103–125.
Liu, X.C., Zhao, Y., Zhao, G.C., Jian, P., Xu, G., 2007. Petrology and geochronology of granulites from the McKaskle Hills, eastern Amery Ice Shelf, Antarctica, and implications for the evolution of the Prydz Belt. J. Petrol. 48, 1443–1470.
Liu, X.C., Jahn, B.M., Zhao, Y., Zhao, G.C., Liu, X.H., 2007. Geochemistry and geochronology of high grade rocks from the Grove Mountains, East Antarctica: evidence for an early Neoproterozoic basement metamorphosed during a single late Neoproterozoic/Cambrian tectonic cycle. Precambr. Res. 158, 93–118.
Liu, X.C., Zhao, Y., Song, B., Liu, J., Cui, J., 2009. SHRIMP U-Pb zircon geochronology of high-grade rocks and charnockites from the eastern Amery Ice Shelf and southwestern Prydz Bay, East Antarctica: constraints on Late Mesoproterozoic to Cambrian tectonothermal events related to supercontinent assembly. Gondwana Res. 16, 342–361.
Liu, X.C., Zhao, Y., Hu, J.M., 2013. The c. 1000-900 Ma and c. 550-500 Ma tectonothermal events in the Prince Charles Mountains-Prydz Bay region, East Antarctica, and their relations to supercontinent evolution. In: Harley, S.L., Fitzsimons, I.C.W., Zhao, Y. (Eds.), Antarctica and Supercontinent Evolution. Geological Society, London, pp. 95–112. Special Publication 283.
Liu, X.C., Jahn, B.M., Zhao, Y., Liu, J., Ren, L.D., 2014. Geochemistry and geochronology of Mesoproterozoic basement rocks from the Eastern Amery Ice Shelf and southwestern Prydz Bay, East Antarctica: implications for a long-lived magmatic accretion in a continental arc. Am. J. Sci. 314, 508–547.
Liu, X.C., Wang, W.-(RZ), Zhao, Y., Liu, J., Chen, H., Cui, Y.C., Song, B., 2016. Early Mesoproterozoic arc magmatism followed by early Neoproterozoic granulite facies metamorphism with a near-isobaric cooling path at Mount Brown, Princess Elizabeth Land, East Antarctica. Precambr. Res. 284, 30–48.
Liu, Y.S., Gao, S., Hu, Z.C., Gao, C.G., Zong, K.Q., Wang, D.B., 2010. Continental and oceanic crust recycling-induced melt-peridotite interactions in the Trans-North China Orogen: U-Pb dating, Hf isotopes and trace elements in zircons of mantle xenoliths. J. Petrol. 51, 537–571.
Ludwig, K.R., 2001. SQUID 1.02: a user's manual. Berkeley Geochronology Center. Special Publication, No. 2.
Ludwig, K.R., 2003. User's manual for Isoplot 3.00. A geochronological Toolkit for Microsoft Excel. Berkeley Geochronology Center. Special Publication, No. 4a.
Manton, W.I., Grew, E.S., Ghofmann, J., Sheraton, J.W., 1992. Granitic rocks of the Jetty Peninsula, Amery Ice Shelf area, East Antarctica. In: Yoshida, Y., Kaminuma, K., Shiraishi, K. (Eds.), Recent Progress in Antarctic Earth Science. Terra Scientific Publishing Company, Tokyo, pp. 179–189.
McKelvey, B.C., Stephenson, N.C.N., 1990. A geological reconnaissance of the Radok Lake area, Amery Oasis, Prince Charles Mountains. Antarct. Sci. 4, 59–69.
Mikhalsky, E.V., 2008. Age of the Earth's crust and the Nd isotopic composition of the mantle sources of East Antarctic Complexes. Geochem. Int. 46, 168–174.
Mikhalsky, E.V., Sheraton, J.W., 2011. The Rayner Tectonic Province of East Antarctica: compositional features and geodynamic setting. Geotectonics 45, 496–512.
Mikhalsky, E.V., Kamenev, I.A., 2013. Recurrent transitional group charnockites in the east Amery Ice Shelf coast (East Antarctica): petrogenesis and implications on tectonic evolution. Lithos 175–176, 230–243.
Mikhalsky, E.V., Sheraton, J.W., Laiba, A.A., Beliatsky, B.V., 1996. Geochemistry and origin of Mesoproterozoic metavolcanic rocks from Fisher Massif, Prince Charles Mountains, East Antarctica. Antarct. Sci. 8, 85–104.
Mikhalsky, E.V., Laiba, A.A., Beliatsky, B.V., Stüwe, K., 1999. Geology, age and origin of the Mount Willing area (Prince Charles Mountains, East Antarctica). Antarct. Sci. 11, 338–352.
Mikhalsky, E.V., Sheraton, J.W., Laiba, A.A., Tingey, R.J., Thost, D.E., Kamenev, E.N., Fedorov, L.V., 2001. Geology of the Prince Charles Mountains, Antarctica. AGSO-Geoscience Australia Bulletin 247, 1–209.
Mikhalsky, E.V., Laiba, A.A., Beliatsky, B.V., 2006. Tectonic subdivision of the Prince Charles Mountains: a review of geologic and isotopic data. In: Fütterer, D.K., Damaske, D., Kleinschmidt, G., Miller, H., Tessensohn, F. (Eds.), Antarctica: Contributions to Global Earth Sciences. Springer-Verlag, Berlin Heidelberg New York, pp. 69–82.
Mikhalsky, E.V., Laiba, A.A., Beliatsky, B.V., 2006. Age and compositional features of rocks from Mt. Meredith and the eastern fringe of the Amery Ice Shelf. Russian Earth Science Research in Antarctica, Collection of Papers 1, 66–93 (in Russian with English abstract).
Mikhalsky, E.V., Sheraton, J.W., Kudriavtsev, I.V., Sergeev, S.A., Kovach, V.P., Kamenev, I.A., Laiba, A.A., 2013. The Mesoproterozoic Rayner Province in the Lambert Glacier area: its age, origin, isotopic structure and implications for Australia-Antarctica correlations. In: Harley, S.L., Fitzsimons, I.C.W., Zhao, Y. (Eds.), Antarctica and Supercontinent Evolution. Geological Society, London, pp. 35–57. Special Publication 283.
Mikhalsky, E.V., Belyatsky, B.V., Presnyakov, S.L., Skublov, S.G., Kovach, V.P., Rodionov, N.V., Antonov, A.V., Saltykova, A.K., Sergeev, S.A., 2015. The geological composition of the hidden Wilhelm II Land in East Antarctica: SHRIMP zircon, Nd isotopic and geochemical studies with implications for Proterozoic supercontinent reconstructions. Precambr. Res. 258, 171–185.

Mikhalsky, E.V., Alexeev, N.L., Belyatsky, B.V., Kapitonov, I.N., Rodionov, N.V., Pogorelskiy, A.I., 2016. The results of preliminary U-Pb dating of zircon from metasedimentary rocks in the Lambert Glacier-Prydz Bay region. Russian Earth Science Research in Antarctica, Collection of Papers 4, 110–141 (in Russian with English abstract).

Möller, A., O'Brien, P.J., Kennedy, A., Kröner, A., 2003. Linking growth episodes of zircon and metamorphic textures to zircon chemistry: an example from the ultrahigh-temperature granulites of Rogaland (SW Norway). In: Vance, D., Müller, W., Villa, I.M. (Eds.), Geochronology: Linking the Isotopic Record with Petrology and Textures. Geological Society, London, pp. 65–81. Special Publications 220.

Morrissey, L.J., Hand, M., Kelsey, D.E., 2015. Multi-stage metamorphism in the Rayner-Eastern Ghats Terrane: P-T–t constraints from the northern Prince Charles Mountains, east Antarctica. Precambr. Res. 267, 137–163.

Morrissey, L.J., Hand, M., Kelsey, D.E., Wade, B.P., 2016. Cambrian high-temperature reworking of the Rayner-Eastern Ghats Terrane: constraints from the northern Prince Charles Mountains region, East Antarctica. J. Petrol. 57, 53–92.

Munksgaard, N.C., Thost, D.E., Hensen, B.J., 1992. Geochemistry of Proterozoic granulites from northern Prince Charles Mountains, East Antarctica. Antarct. Sci. 4, 59–69.

Nichols, G.T., 1995. The role of mylonites in the uplift of an oblique lower crustal section, East Antarctica. J. Metamorph. Geol. 13, 223–228.

Pearce, N.J.G., Perkins, W.T., Westgate, J.A., Gordon, M.P., Jackson, S.E., Neal, C.R., Chenery, S.P., 1996. A compilation of new and published major and trace element data for NIST SRM 610 and NIST SRM 612 glass reference materials. Geostand. Geoanal. Res. 21, 115–144.

Phillips, G., White, R.W., Wilson, C.J.L., 2007. On the role of deformation and fluid during rejuvenation of a polymetamorphic terrane: inferences on the geodynamic evolution of the Ruker Province, East Antarctica. J. Metamorph. Geol. 25, 855–871.

Scrimgeour, I., Hand, M., 1997. A metamorphic perspective on the Pan African overprint in the Amery area of Mac. Robertson Land, East Antarctica. Antarct. Sci. 9, 313–335.

Sengör, A.M.C., Natal'in, B.A., Burtman, V.S., 1993. Evolution of the Altaid tectonic collage and Palaeozoic crustal growth in Eurasia. Nature 364, 299–307.

Sheraton, J.W., Tingey, R.J., Black, L.P., Offe, L., Ellis, D.J., 1987. Geology of Enderby Land and western Kemp Land, Antarctica. BMR Bull. 223, 1–51.

Sheraton, J.W., Tindle, A.G., Tingey, R.J., 1996. Geochemistry, origin, and tectonic setting of granitic rocks of the Prince Charles Mountains, Antarctica. J. Aust. Geol. Geophys. 16, 345–370.

Söderlund, U., Patchett, P.J., Vervoort, J.D., Isachsen, C.E., 2004. The 176Lu decay constant determined by Lu–Hf and U-Pb isotope systematics of Precambrian mafic intrusions. Earth Planet. Sci. Lett. 219, 311–324.

Stephenson, N.C.N., 2000. Geochemistry of granulite-facies granitic rocks from Battye Glacier, northern Prince Charles Mountains, East Antarctica. Aust. J. Earth Sci. 47, 83–94.

Stephenson, N.C.N., Cook, N.D.J., 1997. Metamorphic evolution of calc-silicate granulites near Battye Glacier, northern Prince Charles Mountains, east Antarctica. J. Metamorph. Geol. 15, 361–378.

Thost, D.E., Hensen, B.J., 1992. Gneisses of the Porthos and Athos Ranges, northern Prince Charles Mountains, East Antarctica: constraints on the prograde and retrograde P-T path. In: Yoshida, Y., Kaminuma, K., Shiraishi, K. (Eds.), Recent Progress in Antarctic Earth Science. Terra Scientific Publishing Company, Tokyo, pp. 93–102.

Vavra, G., Schmid, R., Gebauer, D., 1999. Internal morphology, habit and U-Th–Pb microanalysis of amphibolite-to-granulite facies zircons: geochronology of the Ivrea Zone (Southern Alps). Contrib. Miner. Petrol. 134, 380–404.

Tingey, R.J., 1982. The geologic evolution of the Prince Charles Mountains – an Antarctic Archean cratonic block. In: Craddock, C. (Ed.), Antarctic Geoscience. University of Wisconsin Press, Madison, pp. 455–464.

Tingey, R.J., 1991. The regional geology of Archaean and Proterozoic rocks in Antarctica. In: Tingey, R.J. (Ed.), The Geology of Antarctica. Oxford University Press, Oxford, pp. 1–73.

Vervoort, J.D., Blichert-Toft, J., 1999. Evolution of the depleted mantle: Hf isotope evidence from juvenile rocks through time. Geochim. Cosmochim. Acta 63, 533–556.

Wang, Y.B., Liu, D.Y., Chung, S.-L., Tong, L.X., Ren, L.D., 2008. SHRIMP zircon age constraints from the Larsemann Hills region, Prydz Bay, for a late Mesoproterozoic to early Neoproterozoic tectono-thermal event in East Antarctica. Am. J. Sci. 308, 573–617.

Wang, W., Liu, X.C., Zhao, Y., Zheng, G.G., Chen, L.Y., 2016. U-Pb zircon ages and Hf isotopic compositions of metasedimentary rocks from the Grove Subglacial Highlands, East Antarctica: constraints on the provenance of protoliths and timing of sedimentation and metamorphism. Precambr. Res. 275, 135–150.

Wiedenbeck, M., Allé, P., Corfu, F., Griffin, W.L., Meier, M., Oberli, F., von Quadt, A., Roddick, J.C., Spiegel, W., 1995. Three natural zircon standards for U-Th–Pb, Lu–Hf, trace element and REE analyses. Geostand. Geoanal. Res. 19, 1–23.

Williams, I.S., 1998. U-Th-Pb geochronology by ion microprobe. In: McKibben, M.A., Shanks, W.C., Ridley, W.I. (Eds.), Applications of Microanalytical Techniques to Understanding Mineralizing Processes, Reviews in Economic Geology, 7, pp. 1–35.

Young, D.N., Black, L.P., 1991. U-Pb zircon dating of Proterozoic igneous charnockites from the Mawson Coast, East Antarctica. Antarct. Sci. 3, 205–216.

Young, D.N., Zhao, J.-X., Ellis, D.J., Mcculloch, M.T., 1997. Geochemical and Sr–Nd isotopic mapping of source provinces for the Mawson charnockites, East Antarctica: implications for Proterozoic tectonics and Gondwana reconstruction. Precambr. Res. 86, 1–19.

Zhao, Y., Song, B., Wang, Y.B., Ren, L.D., Li, J.L., Chen, T.Y., 1992. Geochronology of the late granite in the Larsemann Hills, East Antarctica. In: Yoshida, Y., Kaminuma, K., Shiraishi, K. (Eds.), Recent Progress in Antarctic Earth Science. Terra Scientific Publishing Company, Tokyo, pp. 155–161.